©2013 Society of Economic Geologists, Inc.
Economic Geology, v. 108, pp. 1793–1811

Segregation and Fractionation of Magmatic Ni-Cu-PGE Sulfides in the Western Jinchuan Intrusion, Northwestern China: Insights from Platinum Group Element Geochemistry

Lie-Meng Chen,[1] Xie-Yan Song,[1,†] Reid R. Keays,[2] Yu-Long Tian,[3] Yu-Shan Wang,[3] Yu-Feng Deng,[1] and Jia-Fei Xiao[1]

[1] *State Key Laboratory of Ore Deposit Geochemistry, Institute of Geochemistry, Chinese Academy of Sciences, 46th Guanshui Road, Guiyang 550002, P. R. China*

[2] *School of Geosciences, Monash University, Victoria 3800, Australia*

[3] *Jinchuan Group Ltd., Jinchang, Gansu 737100, P. R. China*

Abstract

The Jinchuan Ni-Cu-(PGE) deposit is one of the world's largest magmatic sulfide deposits. Recent studies have suggested that the Jinchuan intrusion originally comprised two individual intrusions, the Eastern and the Western intrusions. The Western intrusion consists of an Upper and a Lower unit. The Upper unit is largely free of sulfides with weakly disseminated sulfides only at the base of the unit; these sulfides are characterized by moderate Cu/Pd ratios of 5,500 to 14,900 and relatively high PGE tenors (PGE in 100% sulfides) in the range of 510 to 1,000 ppb Ir_{sul}, 420 to 1,200 ppb Ru_{sul}, and 2,900 to 8,000 ppb Pd_{sul}. Disseminated, net-textured and minor massive sulfides in the Lower unit comprise the No. 24 orebody, the third largest at Jinchuan. The disseminated ores have remarkably high Cu/Pd ratios (24,200–85,600) and low PGE tenors in the range of 120 to 560 ppb Ir_{sul}, 100 to 480 ppb Ru_{sul}, and 430 to 3,600 ppb Pd_{sul}. The net-textured and massive ores contain high IPGE contents (240–820 ppb Ir_{sul} and 170–630 ppb Ru_{sul}) and Ni/Cu ratios (1.7–11.3), low Pd/Ru ratios (0.53–3.1), and exhibit significant Pt depletion (<300 ppb Pt_{sul}). Additionally, small Cu-rich orebodies occur at the base of the No. 24 orebody or in small intrusions within footwall schists, marbles, and granites beneath the Western intrusion. The Cu-rich sulfides have very low IPGE tenors (1.9–16 ppb Ir_{sul} and 6.4–21 ppb Ru_{sul}), and Ni/Cu ratios (0.3–2.8), high Pd/Ru ratios (37.3–378), and highly variable Pt_{sul} between 43 and 11,000 ppb. The PGE geochemistry and model calculations indicate that the disseminated sulfides of the Upper and Lower units segregated from PGE-undepleted and -depleted parental magmas, respectively. The PGE-depleted magma had undergone a minor amount of earlier sulfide liquid extraction at depth. Furthermore, this PGE-depleted parental magma had slightly higher PGE contents than the magma from which the sulfides of the Nos. 1 and 2 orebodies in the Eastern intrusion segregated. The significant variations in base and precious metal ratios of the net-textured and massive sulfide ores are attributed to fractionation of the sulfide melts that formed these ores. This led to both migration of the residual Cu-rich sulfide melts away from the early-formed monosulfide solid solution (mss) to form Cu-rich ores as well as back intrusion of the Cu-rich ores into the mss. The negative Pt anomalies of the net-textured and massive sulfides resulted from preferential extraction of Pt into the Cu-rich residual melts due to the presence of As, Te, and Bi.

Introduction

The Jinchuan Ni-Cu-(PGE) deposit, which occurs at the southwestern margin of the North China craton (Fig. 1), contains more than 500 million metric tons (Mt) of sulfide ore with average grades of 1.06 wt % Ni and 0.7 wt % Cu (Sixth Geological Unit, 1984; Chai and Naldrett, 1992a). The Jinchuan intrusion consists of four elongate ultramafic segments. Structural, lithological, and geochemical studies have shown that these segments belong to two individual intrusions separated by the NNE-SSW–trending fault $F_{16\text{-}1}$, named as the Western and Eastern intrusions (Song et al., 2012). Two largest orebodies (Nos. 1 and 2) are hosted in the Eastern intrusion, while the third largest orebody (No. 24) is situated in the Western intrusion. Most authors (e.g., Tang and Li, 1995; de Waal et al., 2004; Li et al., 2004; Song et al., 2006; Su et al., 2008; Chen et al., 2009b) have suggested that the Jinchuan intrusion and its orebodies are the products of multiple injections of olivine-bearing crystal mushes followed by sulfide-laden crystal mushes from a deep-seated staging magma chamber. Furthermore, Song et al. (2009) proposed that the parental magma of the Nos. 1 and 2 orebodies had experienced segregation of a small proportion of sulfide liquid before entering the staging chamber, which is a part of a magma conduit system. As a result, the sulfides of these orebodies have low PGE contents.

Although Song et al. (2012) proposed that the Lower and Upper units of the Western intrusion formed by different pulses of magma, sulfide segregation processes in the two units and chalcophile element differentiation in the Lower unit have still not been well constrained. Our data show that the sulfides of the two units have distinct chalcophile element compositions and Cu/Pd ratios. These data indicate that the sulfides of the Upper and Lower units segregated from PGE-undepleted and -depleted magmas, respectively. In addition, large variations in PGE tenors of sulfides in the Lower unit suggest fractionation of the sulfide melts and migration of the residual sulfide liquids.

Geologic Background

The Jinchuan ultramafic intrusion, recently dated at Neoproterozoic (827 ± 8 Ma, Li et al., 2005; 833 ± 35 Ma, Yang et al., 2008; 831.8 ± 0.6 Ma, Zhang et al., 2010), is situated in the

† Corresponding author: e-mail, songxieyan@vip.gyig.ac.cn

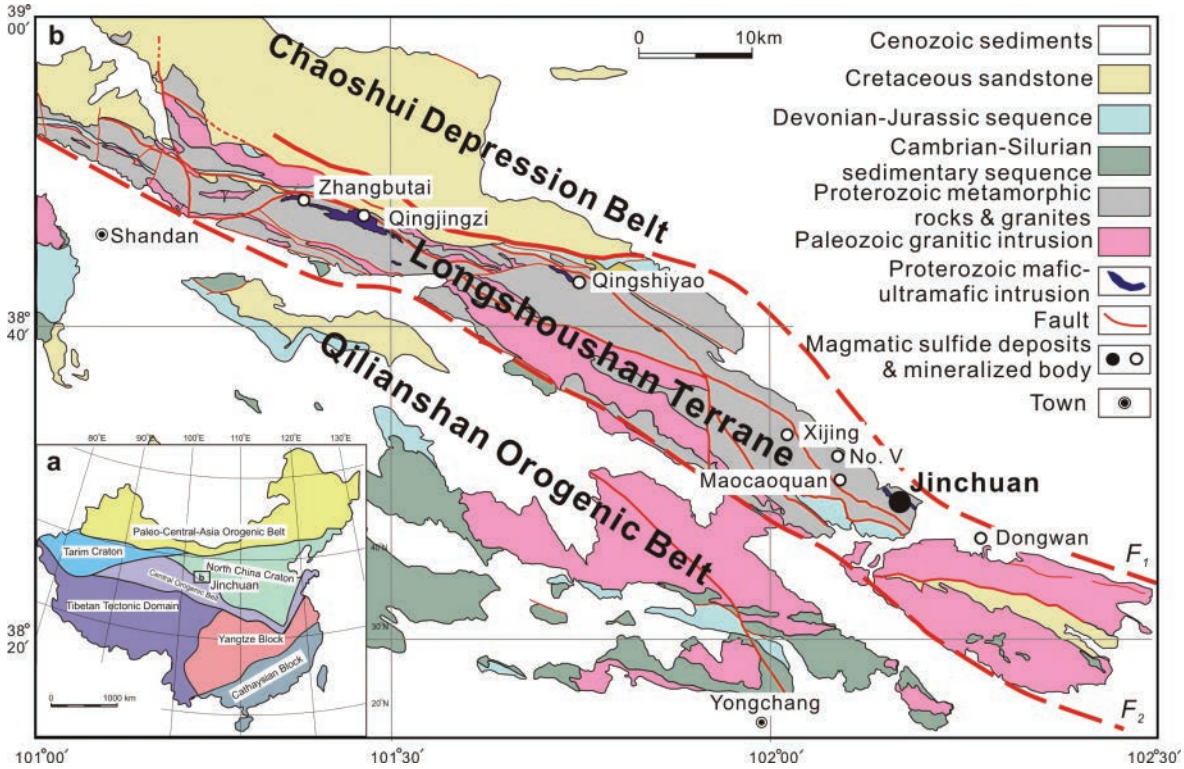

FIG. 1. (a). The main tectonic units of China. (b). Simplified regional geologic map showing locations of the Jinchuan intrusion and several other mafic-ultramafic intrusions in the Longshoushan terrane, which is located at the southwestern margin of the North China craton. Modified after Sixth Geological Unit (1984) and Song et al. (2009).

NW-striking Longshoushan terrane, which is located at the southwestern margin of the North China craton (Fig. 1; Tang and Li, 1995; Zhou et al., 2002). In the Longshoushan terrane, Neoproterozoic and Paleozoic conglomerates, sandstones, and limestones unconformably overlie Paleo-Mesoproterozoic metamorphic units. Many sulfide-mineralized intrusions (e.g., Jinchuan, Zangbutai, and Qingjingzi) and unmineralized intrusions (e.g., Qingshiyao, Xijing, Maocaoquan, and Dongwan) occur in the Longshoushan terrane (Fig. 1b; Sixth Geological Unit, 1984).

The NW-SE-trending Jinchuan intrusion is ~6,500 m long and varies from 20 to ~500 m in width. It was emplaced into Paleo-Mesoproterozoic metamorphic gneisses, schists, marbles, and granites and dips 50° to 80° to the southwest (Fig. 2; Sixth Geological Unit, 1984; Tang and Li, 1995). The intrusion is divided by a series of NE-trending strike-slip faults into segments III, I, II, and IV from west to east (Fig. 2). Song et al. (2012) proposed that the segments on either side of fault $F_{16\text{-}1}$ belong to two independent intrusions, the Eastern and Western intrusions.

The Western intrusion on the west side of fault $F_{16\text{-}1}$ is further divided into Segments I and III by fault F_8 (Fig. 2a). It comprises two megacyclic units termed the Lower and Upper units, which have different lithologic features and are separated by sharp contacts (Fig. 2b; Song et al., 2012). The dominant mineral in the Upper unit rocks is cumulus olivine, which varies in size from 0.5 to 3 mm, together with lesser amounts of clinopyroxene and minor amounts of orthopyroxene. From the base to its top, the Upper unit comprises fine-grained dunite, lherzolite, and minor pyroxenite as olivine decreases and pyroxene increases gradually upward (Fig. 2b). The clinopyroxene is present as oikocrysts that enclose some of the cumulus olivine, and thus these rocks are olivine orthocumulates with poikilitic clinopyroxene (Fig. 3a; cf. Wager et al., 1960). For the Lower unit, the basal rocks are coarse-grained olivine-sulfide cumulates in which the olivine grains normally range from 4 to 7 mm in size (but can be up to 10 mm diam). The olivine-sulfide cumulates are overlain by coarse-grained lherzolite and sometimes have small amounts of pyroxenite at the base of the unit (Fig. 2b). The olivine grains in these rocks are in contact with each other or isolated from each other by sulfides or included in large oikocrysts of clinopyroxene (Fig. 3b-c). Marble xenoliths of variable sizes occur in the Lower unit (Fig. 2b, Sixth Geological

FIG. 2. (a). Geologic map of the Jinchuan intrusion and cross sections of II-14 and II-36 in segment II, showing concentric lithologic zonation in the west part of the Eastern intrusion. (b). Cross section of the Western intrusion; cross section of the exploration lines of III-5 in segment III and I-24, I-16, and I-6 in segment I; and Cu-rich orebody beneath the intrusion found during underground exploration. Samples of this study are collected from ZK 71 (JC06-201 to JC06-248), ZK59 (ZK59-1 to ZK59-25), Location A (JC06-801 to JC06-804), Location B (JC06-806 to JC06-820), Location C (JC06-821 to JC06-822), Location D (I24-1 to I24-7), Location E (JC06-JC06-823), and Location F (L07-1 to L07-14). Modified after Sixth Geological Unit (1981, 1984), Jinchuan Nonferrous Metal Corporation (1997, 2003), Tang and Li (1995), and Song et al. (2009).

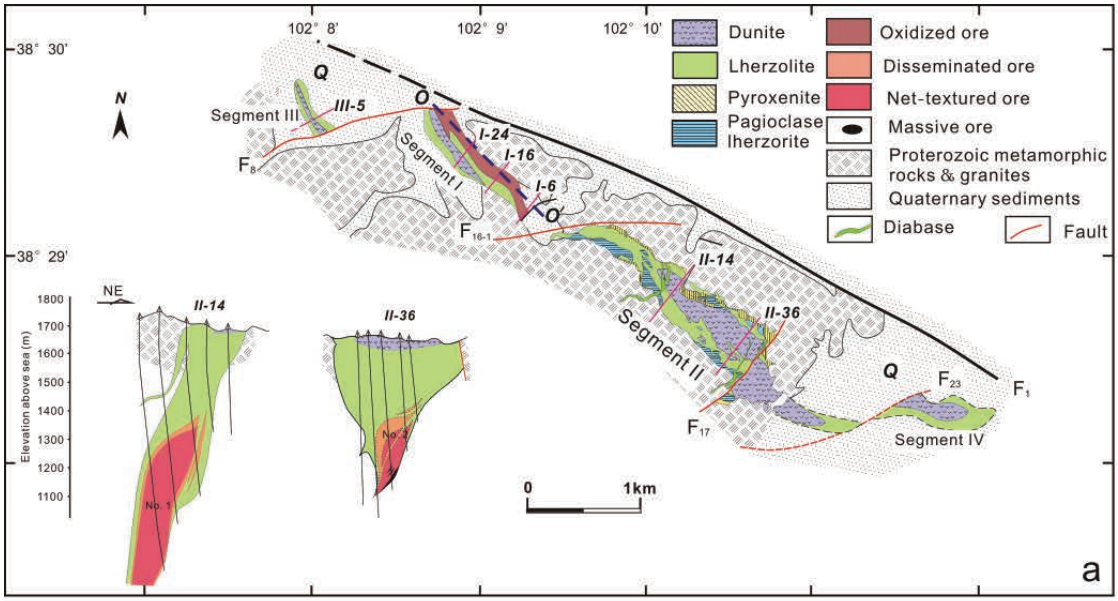
102° 8'
102° 9'
102° 10'
38° 30'
38° 29'
N
Segment III
III-5
Segment I
I-24
I-16
I-6
Segment II
II-14
II-36
Segment IV
F8
F16-1
F17
F23
F1
Q
O
O'
Dunite
Lherzolite
Pyroxenite
Pagioclase lherzolite
Oxidized ore
Disseminated ore
Net-textured ore
Massive ore
Proterozoic metamorphic rocks & granites
Quaternary sediments
Diabase
Fault
NE
Elevation above sea (m)
1800
1700
1600
1500
1400
1300
1200
1100
No. 1
No. 2
0
1km
a

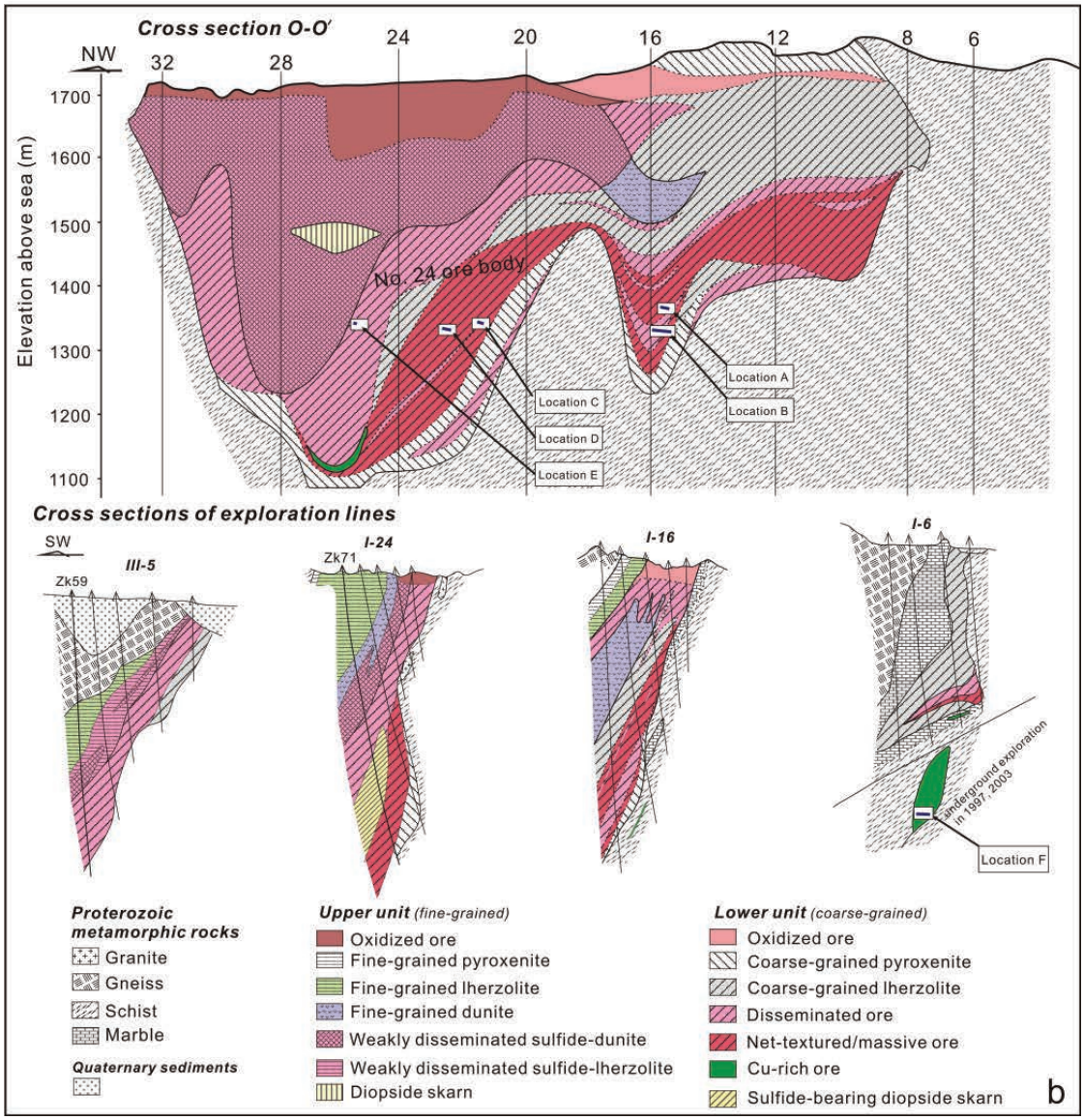
Cross section O-O'
NW
32
28
24
20
16
12
8
6
Elevation above sea (m)
1700
1600
1500
1400
1300
1200
1100
No. 24 ore body
Location A
Location B
Location C
Location D
Location E
Cross sections of exploration lines
SW
III-5
Zk59
I-24
Zk71
I-16
I-6
underground exploration in 1997, 2003
Location F
Proterozoic metamorphic rocks
Granite
Gneiss
Schist
Marble
Quaternary sediments
Upper unit (fine-grained)
Oxidized ore
Fine-grained pyroxenite
Fine-grained lherzolite
Fine-grained dunite
Weakly disseminated sulfide-dunite
Weakly disseminated sulfide-lherzolite
Diopside skarn
Lower unit (coarse-grained)
Oxidized ore
Coarse-grained pyroxenite
Coarse-grained lherzolite
Disseminated ore
Net-textured/massive ore
Cu-rich ore
Sulfide-bearing diopside skarn
b

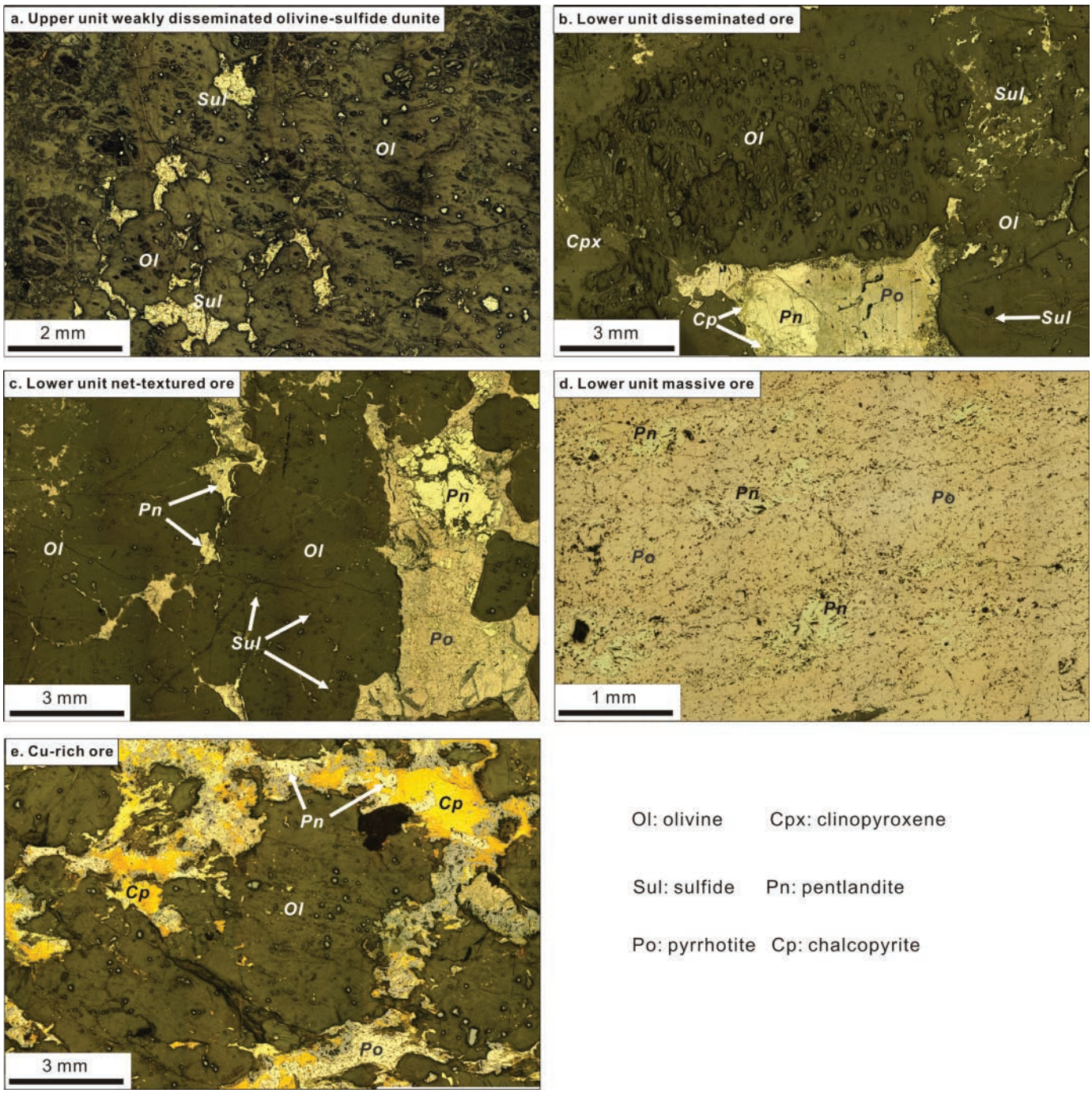

FIG. 3. Microphotographs showing olivine and sulfide textures in sulfides of the Western intrusion at Jinchuan.

Unit, 1984; Tang and Li, 1995; Lehmann et al., 2007; Song et al., 2012).

The Eastern intrusion on the east side of fault $F_{16\text{-}1}$ is divided into Segments II and IV by fault F_{23} (Fig. 2a). It is characterized by a concentric distribution of rock types in the western portion of the Eastern intrusion, where the very large No. 1 orebody comprised of net-textured and disseminated olivine-sulfide cumulate is enveloped by lherzolite. The eastern part of the Eastern intrusion consists of medium- to coarse-grained olivine-sulfide cumulate, sulfide-lherzolite that constitutes the No. 2 orebody, and sulfide-barren lherzolite (Fig. 2a, Sixth Geological Unit, 1984; Song et al., 2009).

Sulfide Mineralization in the Western Intrusion

The No. 24 orebody occurs in the Lower unit of the Western intrusion and consists of net-textured sulfides that give way upward to disseminated sulfides (Fig. 2b). The Upper unit is generally sulfide poor except for weakly disseminated sulfides that occur at its base. The tabular shaped No. 24 orebody is ~1,300 m long and ~20 to 70 m wide, and dips to

depths of 300 to 500 m southwestward. Its thickness is highly variable, generally ranging from ~20 to 100 m but up to 170 m in some locations where the footwall metamorphic rocks are at greater depths (Fig. 2b). The orebody usually occurs above the basal pyroxenite but may be in contact with the footwall metamorphic rocks where the basal pyroxenite is absent (Fig. 2b, Sixth Geological Unit, 1984).

Four main types of sulfide mineralization occur in the Western intrusion:

1. Weakly disseminated sulfides at the base of the Upper unit: This type of mineralization contains <5 modal % sulfides and occurs in the dunite of Segment I and in both the dunite and lherzolite of Segment III (Fig. 2b). The sulfides are interstitial between olivine and pyroxene grains and are composed of pyrrhotite, pentlandite, and minor chalcopyrite (Fig. 3a).
2. Disseminated sulfides in the Lower unit: This is the dominant type of economic mineralization of the No. 24 orebody. The disseminated sulfide zone is thin in the eastern portion of Segment I but becomes thicker to the west and extends into Segment III (Fig. 2b). The disseminated ores generally contain 3 to 15 modal % sulfides, which include 1 to 8 modal % pyrrhotite, 1 to 5 modal % pentlandite, and 1 to 3 modal % chalcopyrite (Fig. 3b). In addition, the disseminated ore assemblages contain 0.1 to 1.2 modal % magmatic magnetite, which are enclosed in silicate crystals or interstitial between them (Sixth Geological Unit, 1984).
3. Net-textured sulfides in the Lower unit: This is a major type of mineralization of the No. 24 orebody and occurs beneath the disseminated ores. It is very thick (up to 60 m wide) between exploration lines 8 and 24 in Segment I, but thins to the west and is absent in Segment III (Fig. 2b). The net-textured ores contain 15 to 40 modal % sulfides consisting of 10 to 30 modal % pyrrhotite, 4 to 10 modal % pentlandite, and 1 to 4 modal % chalcopyrite (Fig. 3c). In addition, small massive sulfide bodies occasionally occur in the eastern parts of the No. 24 orebody within the net-textured ores. Massive sulfides mainly consist of pyrrhotite (50–70 modal %), pentlandite (10–20 modal %), and only minor chalcopyrite (1–7 modal %; Fig. 3d). In these sulfides, anhedral pentlandite crystals occur between anhedral or subhedral pyrrhotite grains (Fig. 3b-d) or as exsolution flames in pyrrhotite. Both the net-textured and massive sulfides contain significant magmatic magnetite contents, varying from 1.01 to 4.4 modal % (Sixth Geological Unit, 1984).
4. Cu-rich sulfides: These sulfides occur both at the base of the No. 24 orebody (Sixth Geological Unit, 1984) as well as in individual ultramafic intrusions in the Proterozoic metamorphic rocks beneath the eastern portion of the Western intrusion (Jinchuan Nonferrous Metal Corporation, 1997, 2003). The beanpod-shaped bodies are generally several meters thick and tens of meters long. The Cu-rich ores consist of disseminated or net-textured sulfides and are characterized by relatively high chalcopyrite proportions (2–14 modal % chalcopyrite, 5–15 modal % pyrrhotite, and 1–6 modal % pentlandite; Fig. 3e).

Sampling and Analytical Methods

Fifty-seven ultramafic rocks and sulfide ores were collected from borehole ZK71, which was drilled through the middle part of Segment I, and borehole ZK59, which was drilled through the eastern part of Segment III (Fig. 2b). Unfortunately, most of sulfide-rich ores in borehole ZK71 had already been extensively sampled. Consequently, an additional 25 samples of net-textured, massive, and disseminated ores were collected from underground drifts in the No. 24 orebody. Thirteen Cu-rich ores were also collected. The locations of these samples in this study are presented in Figure 2.

Nickel and Cu contents were determined by inductively coupled plasma-optical emission spectrometry (ICP-OES) at the Institute of Geochemistry, Chinese Academy of Sciences. The international reference materials (GSR-1, -2, -3, -4, -5, AMH-1, OU-6, RTS-2, -3, GBPG-1, GBW-1, and GeoPT-12) were used for analytical quality control. The precision is generally better than ± 1% relative standard deviation (RSD) when the Ni and Cu concentrations of the samples are higher than 200 ppm, and 1 to 3% RSD when less than 200 ppm. Arsenic, Te, and Bi contents were determined by ICP-OES at ALS Mineral-ALS Chemex (Guangzhou) Co., Ltd. (http://www.alsglobal.com/minerals/ services.aspx). Whole-rock S contents were measured using a gravimetric method and infrared (IR) absorption in the Geological Analysis Central of the Metallogenic Geology Bureau of Southwest China; the detection limits are ~100 ppm and the accuracies are estimated to be better than ±8% RSD.

The PGE analyses were obtained by isotope dilution (ID)-ICP-MS using the NiS fire assay coupled with the tellurium coprecipitation method of Jackson et al. (1990), with some modifications at the State Key Laboratory of Ore Deposit Geochemistry, Institute of Geochemistry, Chinese Academy of Sciences. The analytical procedures have been described by Qi et al. (2004, 2006). The total procedural blanks and analytical results of Certified Reference Materials (CRM) UMT-1, WPR-1, and TDB-1 used in this study, together with their certified values, are given in Table 1. The analytical results for our samples are listed in Tables 2 and 3. In addition, the data from Song et al. (2006, 2009) and Su et al. (2008) are

TABLE 1. Analytical Quality Control Data for the PGE Analyses

		Ir (ppb)	Ru (ppb)	Rh (ppb)	Pt (ppb)	Pd (ppb)
UMT-1	Expected	8.8 ± 0.6	10.9 ± 1.5	9.5 ± 1.1	129 ± 5	106 ± 3
	This study	9.05	10.6	10.95	142	110.5
WPR-1	Expected	13.5 ± 1.8	21.6 ± 4.3	13.4 ± 0.9	285 ± 12	235 ± 9
	This study	14.8	23.4	13.1	259	244
TDB-1	Expected	0.15	0.3	0.7	5.8 ± 1.1	22.4 ± 1.4
	This study	0.13	0.34	0.52	5.03	22.0
Blank[1]		0.04	0.08	0.03	0.30	0.56

[1] Blank value is expressed as concentrations in 10-g sample

TABLE 2. Concentrations of S, Ni, Cu, and PGE of Samples from Boreholes ZK71 and ZK59, the Western Intrusion, and Its Hosting Orebody at Jinchuan

Location	Rocks	Sample no.	Depth (m)	S (wt %)	Ni (wt %)	Cu (wt %)	Ir (ppb)	Ru (ppb)	Rh (ppb)	Pt (ppb)	Pd (ppb)	Ni/Cu	Cu/Pd (*1,000)
ZK71													
Upper unit (Fine-grained)	Lherzolite	JC06-216	5	0.05	0.18	0.02	4.54	3.91	1.73	13.3	18.9	7.59	12.8
		JC06-207	30	0.11	0.13	0.01	1.78	1.44	0.66	21.3	9.6	12.9	10.5
		JC06-206	36.5	0.05	0.13	0.01	1.51	1.28	0.51	14.1	9.0	10.8	12.9
		JC06-202	48	0.15	0.18	0.05	5.83	4.57	2.25	83.3	35.4	3.93	12.8
		JC06-201	51	0.15	0.18	0.06	5.67	4.93	2.28	69.7	37.4	3.16	15.6
		JC06-220	66	0.44	0.23	0.11	8.55	8.67	4.30	139	69.9	2.15	15.6
		JC06-209	81	0.11	0.15	0.03	2.77	2.19	2.06	38.2	14.1	5.38	19.3
		JC06-213	95	0.11	0.12	0.01	1.21	1.11	0.43	11.5	6.0	19.4	10.6
		JC06-227	107	0.35	0.17	0.05	5.41	4.87	2.22	57.3	36.6	3.74	12.5
		JC06-214	118	0.14	0.18	0.06	6.61	5.52	2.90	71.1	40.1	3.21	14.2
		JC06-221	129	0.34	0.27	0.14	12.4	10.1	5.41	161	86.3	1.96	15.9
		JC06-222	138	0.17	0.16	0.05	6.16	4.82	2.64	72.3	33.7	3.06	15.2
		JC06-212	148	0.21	0.17	0.04	5.18	4.13	2.02	48.1	31.3	4.42	12.6
		JC06-223	157	0.36	0.14	0.02	1.67	1.44	0.63	16.8	12.8	7.41	14.8
		JC06-244	176	0.23	0.28	0.08	13.1	12.1	6.18	176	91.8	3.26	9.20
	Weakly disseminated sulfide dunite	JC06-245	187	0.59	0.28	0.06	12.1	11.1	5.69	173	86.1	4.91	6.57
		JC06-245[1]	187	0.59	0.28	0.06	14.5	10.6	5.02	157	80.9	4.91	7.00
		JC06-246	197	0.17	0.19	0.02	6.61	5.61	2.35	69.0	37.6	9.22	5.50
		JC06-242	210	0.37	0.24	0.07	8.94	7.47	3.96	119	55.2	3.55	12.1
		JC06-248	230	0.72	0.50	0.47	18.4	16.8	9.6	358	167	1.06	28.1
		JC06-237	262	1.20	0.50	0.18	28.6	21.8	13.2	387	194	2.75	9.40
		JC06-234	278.5	1.04	0.61	0.33	22.5	34.5	18.1	410	220	1.87	14.9
		JC06-236	292	1.13	0.38	0.25	15.5	12.7	8.31	366	219	1.52	11.5
Lower unit (Coarse-grained)	DS-dunite	JC06-232	316	1.65	0.45	0.29	9.8	8.42	4.55	168.1	98.1	1.56	29.6
		JC06-233	333	1.69	0.49	0.30	12.4	11.0	5.6	201.3	94.9	1.62	31.8
		JC06-229	382	2.87	0.75	0.72	12.7	19.8	10.5	512.9	266	1.03	27.2
	Diospide skarn	JC06-238	411	1.83	0.48	0.56	5.22	9.27	4.73	854	213	0.85	26.2
		JC06-239	428	1.33	0.34	0.15	10.8	9.89	4.83	202	86.0	2.30	17.1
		JC06-230	439	0.58	0.34	0.10	0.19	0.31	0.10	1.81	3.04	3.38	332
		JC06-240	459	0.20	0.23	0.12	3.39	3.14	1.35	59.3	25.9	1.85	47.2
	DS-lherzolite	JC06-224	524	2.18	0.56	0.60	13.8	15.9	7.08	451	162	0.94	37.2
		JC06-226	542	4.27	1.27	0.75	20.0	15.3	7.31	276	234	1.70	32.0
		JC06-225	560	3.65	0.87	0.28	20.4	18.4	7.72	206	105	3.07	27.1
		JC06-231	571	1.80	0.55	0.20	7.00	5.81	3.41	233	55.3	2.74	36.1
		JC06-204	585	0.06	0.12	0.02	0.01	0.03	0.29	6.53	11.4	5.40	19.5
ZK59													
Upper unit (Fine-grained)	Lherzolite	ZK59-06	304	0.16	0.14	0.02	2.84	2.54	1.14	32.9	14.1	5.85	17.5
		ZK59-09	315	0.13	0.12	0.02	0.88	0.84	0.29	12.7	3.6	5.60	59.7
		ZK59-08	330	0.14	0.13	0.01	2.39	1.85	0.86	45.6	10.0	11.03	11.7
	Weakly disseminated sulfide dunite	ZK59-05	356	0.51	0.28	0.08	14.1	10.75	5.86	162	81.8	3.40	10.1
		ZK59-04	372	0.34	0.21	0.05	9.00	6.09	3.27	89.0	44.4	3.78	12.3
		ZK59-02	400	0.22	0.21	0.04	8.09	6.20	4.15	109	58.6	5.68	6.3
		ZK59-01	410	0.13	0.10	0.004	19.6	14.31	7.79	296	98.6	28.61	0.4
		ZK59-27	427	1.26	0.46	0.11	20.1	15.15	7.19	288	96.7	4.12	11.5

TABLE 2. *(Cont.)*

Location	Rocks	Sample no.	Depth (m)	S (wt %)	Ni (wt %)	Cu (wt %)	Ir (ppb)	Ru (ppb)	Rh (ppb)	Pt (ppb)	Pd (ppb)	Ni/Cu	Cu/Pd (*1,000)
Lower unit (Coarse-grained)	DS-lherzolite	ZK59-25	455	1.89	0.66	0.42	14.4	12.5	5.09	94.9	60.7	1.57	69.2
		ZK59-24	471	1.84	0.64	0.27	16.1	14.5	6.08	221	86.1	2.37	31.3
		ZK59-23	488	1.02	0.28	0.26	15.5	12.7	5.93	216	89.1	1.08	29.2
		ZK59-22	500	1.99	0.66	0.29	10.9	8.19	4.29	105	46.1	2.28	62.9
		ZK59-21	509	1.71	0.5	0.41	9.60	7.66	4.14	231	91.6	1.22	44.7
		ZK59-20	521	2.51	0.56	0.84	17.7	16.0	6.37	403	143	0.67	58.6
		ZK59-20[1]	521	2.51	0.56	0.84	18.7	16.5	6.36	398	144	0.67	58.2
		ZK59-10	539	2.55	0.78	1.01	10.6	12.7	5.04	765	258	0.77	39.2
		ZK59-18	565	2.44	0.84	0.5	22.7	21.4	8.59	443	172	1.68	29.0
		ZK59-17	580	3.72	1.05	1.46	15.0	11.8	6.55	419	265	0.72	55.1
		ZK59-15	595	2.35	0.61	0.68	18.3	14.4	5.62	329	95.7	0.90	71.1
		ZK59-12	624	3.27	0.49	0.9	14.8	12.3	5.38	143	37.7	0.54	239
		ZK59-13	635	2.51	0.68	0.21	9.60	7.20	3.04	249	75.9	3.24	27.7
		ZK59-16	658	2.18	0.50	0.83	8.58	5.97	3.36	329	96.9	0.60	85.6
		ZK59-19	668	3.08	0.86	0.56	15.0	12.6	6.20	262	155	1.54	36.2

Abbreviations: DS = disseminated sulfide,
[1] Samples are duplicate

compared in the following discussion. The calculation of the chalcophile element in 100% sulfides (= the metal tenors of the sulfides) was done following the procedure described by Naldrett and Duke (1980) and Song et al. (2009); these are expressed, for example, as Ni_{sul}. Samples with less 0.5 wt % S were eliminated from the tenor calculations.

Analytical Results

The Upper unit of the Western intrusion has quite similar chalcophile element compositions in Segments I and III. Nickel, Cu, and the PGE all decrease upward in the Upper unit in both Segments I and III as illustrated by data for boreholes ZK71 and ZK59, respectively (Table 2, Fig. 4a-b). The weakly disseminated sulfides in the Upper unit have total PGE contents varying from 706 to 121 ppb. Both the sulfide-barren lherzolite and samples with weakly disseminated sulfides have low Cu/Pd ratios from 9,200 to 15,900 and from 5,500 to 14,900 (except for a few samples), respectively, as well as Ni/Cu ratios of 1.1 to 9.2. The chalcophile elements correlate positively with S in the rocks with weakly disseminated sulfides, but not in the sulfide-barren lherzolite (Fig. 5). These samples have moderate Ni and Cu tenors and high PGE tenors (510–1,000 ppb Ir_{sul}, 420–1,200 ppb Ru_{sul}, and 2,900–8,000 ppb Pd_{sul}). The PGE tenors of these sulfides are generally well correlated (Fig. 6), indicating that these metals have not been modified by hydrothermal processes.

Compared with the weakly disseminated sulfides in the Upper unit, the disseminated sulfides of the No. 24 orebody in the Lower unit have higher Cu/Pd ratios (24,200–85,600) and lower PGE tenors (e.g., 120–560 ppb Ir_{sul}, 100–480 ppb Ru_{sul}, and 430–3,600 ppb Pd_{sul}; Fig. 6). The well positive correlations between Ru and Ir, Pt, and Pd suggest limited modification of the PGE in these sulfides by hydrothermal processes (Fig. 6c-e). On the other hand, the disseminated sulfides of the No. 24 orebody have Pd/Ru and Pt/Pd ratios and primitive mantle normalized chalcophile element patterns similar to those of the weakly disseminated sulfides in the Upper unit (Figs. 6e, f, 7a). Moreover, the very narrow Pd/Ru (and Pd/Ir) ratios of both the disseminated sulfides of the No. 24 orebody (Pd/Ru = 3.5–20.9) and the weakly disseminated sulfides in the Upper unit (Pd/Ru = 6.4–17.3) suggest that the sulfides have not experienced extensive fractional crystallization of sulfide liquid. The tenors of the disseminated sulfides in the No. 24 orebody are lower than those of Noril'sk-Talnakh (Russia) and are slightly higher than those of Voisey's Bay (Canada), but comparable with those of the Eagle deposit in the United States (Fig. 7d; Barnes and Maier, 1999; Naldrett et al., 2000; Ding et al., 2012; Lightfoot et al., 2012).

The net-textured and massive sulfides of the No. 24 orebody exhibit strong positive correlations between Ni, Ir, and Ru versus S (Fig. 5a, c, d), but weak correlations between Cu, Pt, and Pd versus S (Fig. 5b, e, f). They are distinguished from the disseminated sulfides by generally higher Ni/Cu ratios (1.7–11.3), slightly higher Ir_{sul} (240–820 ppb), and Ru_{sul} (170–630 ppb), but markedly lower Pd_{sul} (<1,000 ppb) and Pt_{sul} (<300 ppb; Fig. 6). As a result, they display notable Ir-group PGE enrichment and Pt depletion metal patterns on a primitive mantle normalized basis (Fig. 7b).

In contrast with the net-textured and massive sulfides, the Cu-rich sulfides are characterized by low Ir_{sul} (1.9–16 ppb) and

TABLE 3. Concentrations of S, Ni, Cu, PGE, As, Bi, and Te of Samples from the Underground Drifts, the Western Intrusion, and Its Hosting Orebody at Jinchuan

Location	Ore types	Sample no.	S (wt %))	Ni (wt %)	Cu (wt %)	Ir (ppb)	Ru (ppb)	Rh (ppb)	Pt (ppb)	Pd (ppb)	As (ppm)	Bi (ppm)	Te (ppm)	Ni/Cu (ppb)	Cu/Pd (*1,000)
Location A in Figure 2b (1,320-m level, exploration line 16)	MS	JC06-801	24.7	4.96	1.63	211	207	97.7	60.9	219	4.90	3.89	2.71	3.04	74.7
		JC06-802	20.9	4.23	1.97	238	91.7	78.7	102	1216	3.90	1.49	5.07	2.15	16.2
		JC06-803	32.2	6.11	1.60	313	504	159	83.8	570	5.60	2.06	1.98	3.81	28.1
		JC06-804	33.6	6.09	2.40	220	354	123	35.8	187	5.40	1.43	1.79	2.54	128
Location B in Figure 2b (1,313-m level, exploration line 16)	MS	JC06-806	32.7	5.94	1.50	570	537	168	59.6	579	4.8	3.39	2.68	3.97	25.8
		JC06-807	31.5	6.16	2.36	520	444	191	12.8	628	3.6	1.58	1.75	2.61	37.6
		JC06-808	31.4	5.95	1.71	392	420	168	41.7	467	3.7	1.7	2.15	3.48	36.5
		JC06-809	29.7	5.70	2.12	604	496	202	11.6	731	3.5	2.34	2.46	2.69	29.0
		JC06-811	30.7	6.92	2.02	665	503	201	53.3	676	4.7	0.88	1.96	3.43	29.8
		JC06-818	34.0	6.59	1.10	404	364	161	30.3	350	9.0	2.72	2.38	6.00	31.4
	DS	JC06-812	1.53	0.39	0.29	5.09	4.20	2.50	141	87.7	n.d.	n.d.	n.d.	1.38	32.6
		JC06-813	3.64	1.26	0.30	27.5	16.6	7.36	35.8	121.9	n.d.	n.d.	n.d.	4.27	24.2
		JC06-814	2.87	0.72	0.58	28.4	21.5	7.53	200	74.8	n.d.	n.d.	n.d.	1.24	77.5
		JC06-815	3.60	1.00	0.75	26.1	18.4	11.1	676	136	n.d.	n.d.	n.d.	1.33	55.2
Location C[1] in Figure 2b	DS	JC06-821	2.18	0.64	0.66	25.4	18.4	9.22	151	118	n.d.	n.d.	n.d.	0.97	55.6
		JC06-822	5.15	0.71	1.44	19.5	38.3	16.0	748	174	n.d.	n.d.	n.d.	0.49	82.7
Location E[2] in Figure 2b	DS	JC06-823	2.48	0.58	1.00	38.5	33.1	19.5	490	198	n.d.	n.d.	n.d.	0.58	50.4
Location D in Figure 2b (1,313-m level, between exploration lines 23 and 24)	DS	I24-7	3.15	0.88	0.39	12.1	11.1	5.8	117	121	n.d.	n.d.	n.d.	2.26	32.2
	NTS	I24-1	7.32	2.00	0.22	94.5	83.8	27.6	29.9	98.2	5.20	1.38	1.40	9.09	22.4
		I24-2	6.91	1.73	0.83	82.3	88.2	27.2	17.7	116	2.30	1.15	1.12	2.08	71.8
		I24-3	8.11	2.01	1.13	85.5	95.7	27.3	44.3	166	4.80	1.62	2.22	1.78	68.3
		I24-4	8.01	1.36	2.13	117	125	26.5	25.1	144	5.20	0.98	1.83	0.64	148
		I24-5	10.1	2.70	0.42	65.3	58.2	23.8	28.1	179	2.80	1.80	3.18	6.4	23.4
		I24-6	5.32	1.43	0.12	53.5	61.4	18.3	42.5	35.8	2.20	1.03	1.33	11.9	33.6
Location F in Figure 2b (1,160-m level, exploration line of 6)	Cu-rich ore	L07-1	8.86	1.67	4.00	1.25	1.73	1.29	889	304	8.30	7.06	20.4	0.4	132
		L07-2	7.35	1.39	0.3	0.39	1.52	0.71	20.3	461	3.80	5.52	24.4	4.25	92.3
		L07-3	9.24	1.53	0.3	0.69	1.72	0.72	90.3	446	4.80	4.00	13.3	4.60	103
		L07-4	9.03	4.46	1.7	1.35	1.95	1.54	64.3	731	5.40	6.18	10.8	2.65	36.3
		L07-5	8.68	2.64	0.6	0.76	1.66	1.53	144	516	7.30	1.55	7.43	4.16	80.7
		L07-6	8.16	2.88	2.9	1.29	2.26	3.05	47.0	331	6.30	2.41	3.96	0.98	29.6
		L07-7	6.13	0.56	0.5	2.13	1.83	1.17	70.1	172	5.20	1.59	3.36	1.18	68.4
		L07-9	5.89	1.45	0.4	0.69	1.91	1.23	1758	349	6.60	7.73	11.8	3.31	95.0
		L07-10	5.35	1.93	3.3	2.11	2.72	3.44	165.2	288	5.50	1.87	2.79	0.58	20.2
		L07-11	6.04	1.72	1.4	2.31	3.51	5.08	118	131	5.10	1.59	2.35	1.22	93.5
		L07-12	5.79	2.59	2.2	2.09	2.00	2.88	103	329	5.10	1.87	5.14	1.20	36.6
		L07-13	8.99	2.58	1.1	4.01	2.34	4.06	62.1	885	8.50	1.95	9.60	2.36	26.6
		L07-14	10.7	2.64	0.8	1.60	1.89	2.12	12.7	401	5.40	4.19	6.44	3.23	80.5

Abbreviations: DS = disseminated sulfide, NTS = net-textured sulfide, MS = massive sulfide, n.d. = not detected

[1] Location C is located at 1,313-m level, exploration line of 22

[2] Location E is located at 1,313-m level, exploration line of 26

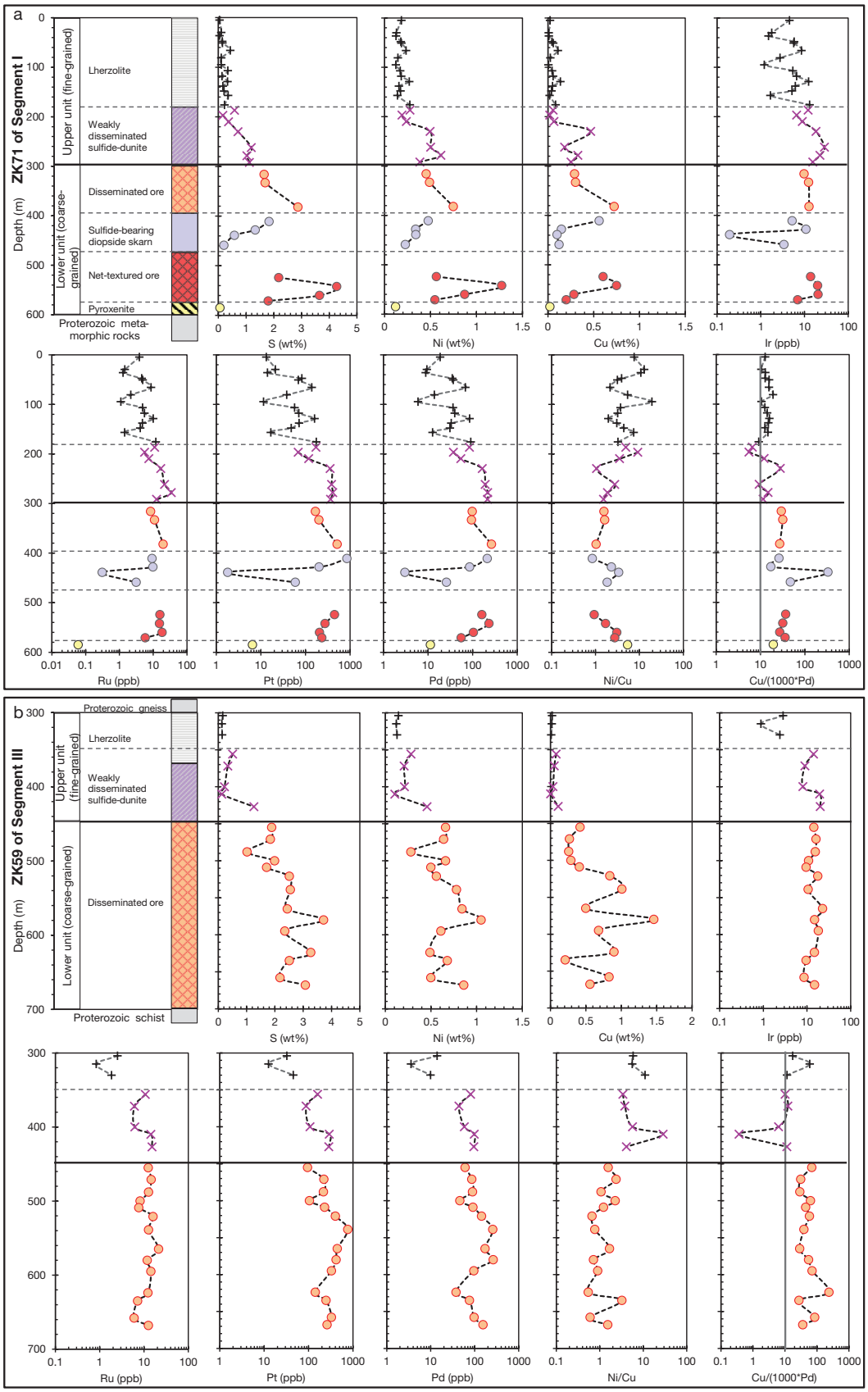

FIG. 4. Variations of S, Ni, Cu, PGE, Ni/Cu, and Cu/(1,000*Pd) ratios with relative stratigraphic position in (a) bore hole ZK71 (Fig. 2b) cross Segment I and (b) bore hole ZK59 (Fig. 2b) across Segment III.

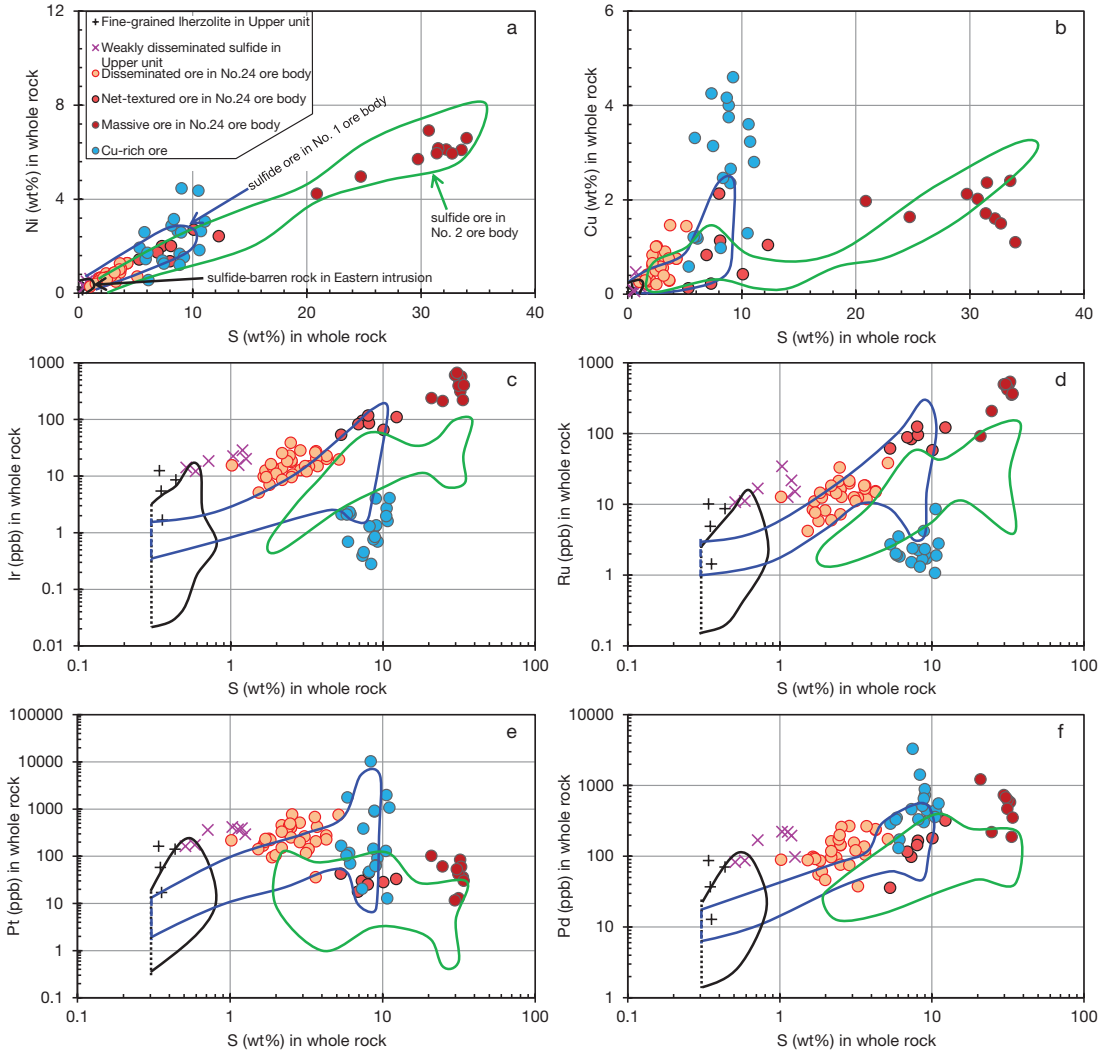

FIG. 5. Variations of S vs. Ni, Cu, Ir, Ru, Pt, and Pd for the samples of the Western and Eastern intrusions. Rocks with less 0.3 wt % S were excluded from the plot. Samples of the Western intrusion are from this study; Cu-rich ores are from this study and Su et al. (2008), and those of the Eastern intrusion are from Song et al. (2006, 2009), and Su et al. (2008).

Ru_{sul} (6.4–21 ppb), large variations in Pt_{sul} (43–11,000 ppb) and enrichment in Cu_{sul} and Pd_{sul} (Fig. 7c), resulting in lower Ni/Cu ratios (0.3–2.8) but much higher Pd/Ru ratios (37.3– 378; Fig. 6a, e). Previously published data show that the highly heterogeneous Cu-rich orebodies at the base of the No. 24 orebody have Pt and Pd contents varying from 1.0 to 82 ppm and from 0.13 to 12 ppm, respectively. Their Pt/Pd ratios range from 3.4 to 12 and average 7.7 (Sixth Geological Unit, 1984); these ratios are significantly higher than those of our samples, which range from 0.03 to 5.0 but are mostly <1 (Fig. 6f). More recently, our new unpublished analyses indicate that their whole-rock Pt concentrations generally vary from 580 to 14,000 ppb (two samples up to 50,000 and 68,000 ppb Pt) and their Pt/Pd ratios range from 3.0 to 44 (Fig. 7c). The Jinchuan Cu-rich sulfides have similar PGE patterns to those of Cu-rich veins in the Noril'sk deposit and are much steeper patterns than those of other sulfides (Fig. 7d; Naldrett et al., 1994; Barnes and Maier, 1999).

The sulfides of the Western and Eastern intrusions have similar Ni and Cu tenors. However, the sulfides of the Western intrusion contain slightly higher whole-rock PGE contents at the same S concentrations relative to those of the Eastern intrusion (Fig. 5). The disseminated sulfides of the Nos. 1 and 2 orebodies in the Eastern intrusion have markedly lower PGE tenors than those of the No. 24 orebody (Fig. 7a) as well as higher Cu/Pd ratios (10,000–548,000, mostly > 30,000; Song et al., 2009). Although the net-textured and massive sulfides of the Nos. 1 and 2 orebodies show similar Pt depletion to those of the No. 24 orebody, they show much larger variations in IPGE than those of the No. 24 orebody (Fig. 7b).

Arsenic, Te, and Bi exhibit broad correlations with Pt and Pd in samples from the No. 24 orebody (Fig. 8). The net-textured and massive sulfides have lower contents of As, Te, and Bi contents on a 100% sulfide basis than the Cu-rich ores. Platinum displays a strong correlation with As and exhibits good correlations with Te and Bi (Fig. 8a-c). One the other hand, Pd shows weak correlations with these elements in all samples (Fig. 8d-f).

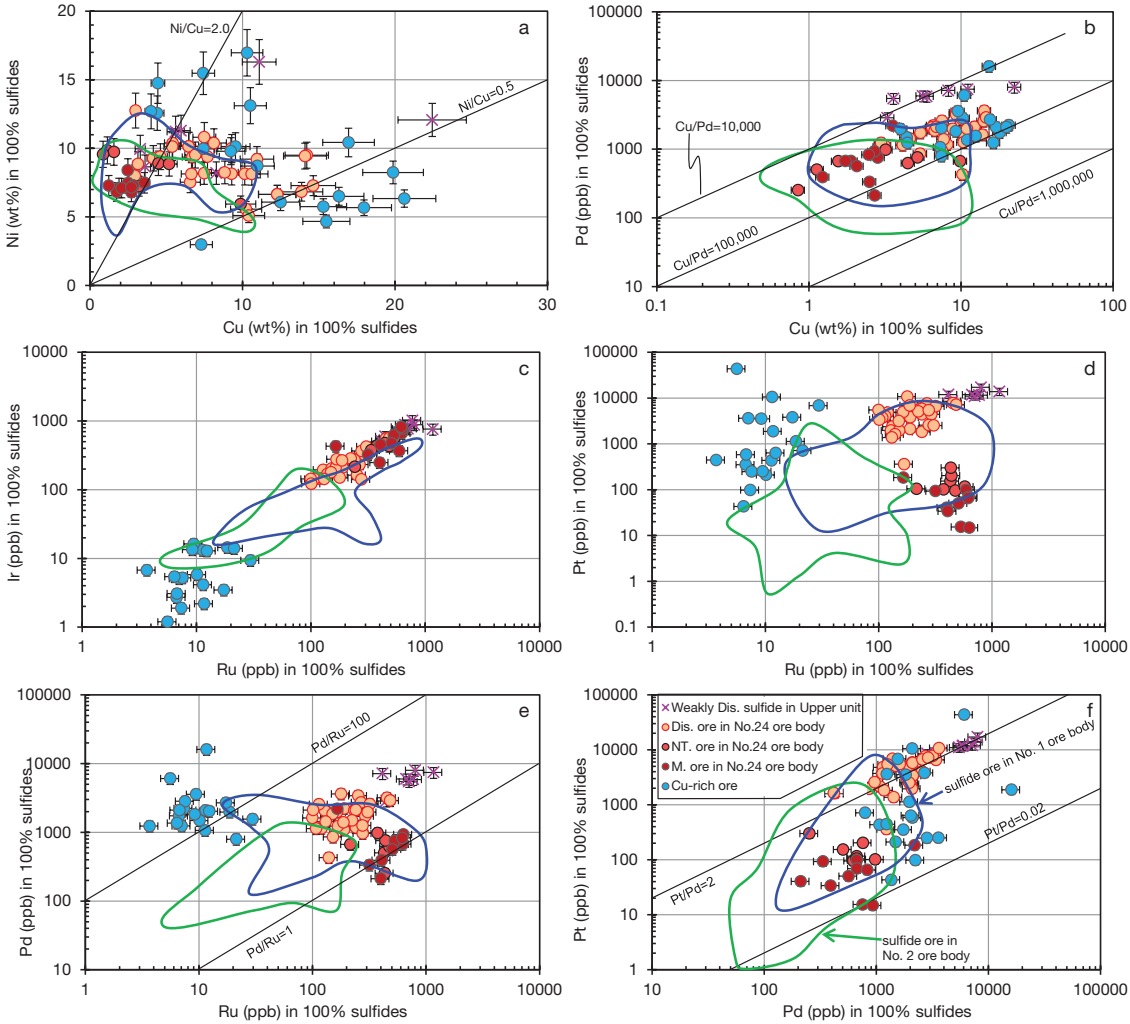

FIG. 6. Variations of Cu vs. Ni and Pd, Ru vs. Ir, Pt, and Pd, and Pt vs. Pd in 100% sulfides for the samples of the Western and Eastern intrusions. Samples of the Western intrusion are from this study; Cu-rich ores are from this study and Su et al. (2008), and those of the Eastern intrusion are from Song et al. (2006, 2009) and Su et al. (2008). The accumulated uncertainties in tenors of these elements are estimated as ~10% for Ni and Cu and ~18% for PGE, according to Kerr (2001). Abbreviations: Dis. ore = disseminated ore, M. ore = massive ore, NT. ore = net-textured ore.

Discussion

As described above, the four types of sulfide mineralization in the Western intrusion are significantly different from the Nos. 1 and 2 orebodies in spatial distribution and chalcophile element compositions. These differences imply that the sulfides of the Western intrusion segregated from distinctly different parental magmas and experienced different fractionation processes to those of the Eastern intrusion. This is important for us to understand more comprehensively the genesis of the Jinchuan deposit.

Nature and chalcophile element compositions of the parental magmas

The compositions of parental magmas play a critical role in the PGE compositions of the sulfides that segregate from them. Chai and Naldrett (1992b) estimated that the parental magma of the Jinchuan intrusion was a high Mg basalt with 11.5 wt % MgO, while Chen et al. (2009b) and Li and Ripley (2011) later estimated that it had 12.3 to 12.6 wt % MgO. On the other hand, Tonnelier (2010) proposed that the parental magma was a ferropicritic magma with >15 wt % MgO and 13 wt % FeO_{total}, which is similar to the ferropicrite flows of the Pechenga area, Russia (Hanski and Smolkin, 1995). The low forsterite contents of olivine in the Jinchuan intrusions (81–86) suggest that the parental magmas were not primary mantle melts but had experienced significant fractional crystallization (Li et al., 2004; Li and Ripley, 2011).

Song et al. (2009) assumed that the Jinchuan parental magma was similar to the Mokulaevsky basalts at Noril'sk (Naldrett et al., 1995; Lightfoot and Keays, 2005). However, because the Jinchuan sulfides contain significantly lower PGE than those of the Noril'sk ores, they speculated that the sulfides of the Nos. 1 and 2 orebodies had segregated from a silicate magma depleted in PGE due to prior weak sulfide separation under R factors of 10^3 to 10^4 (up to 10^5 for modeling Ir contents). These R factors are greater than most magmatic Ni-Cu-(PGE) deposits and are inconsistent with the very large amount of sulfides at Jinchuan (Tonnelier, 2010).

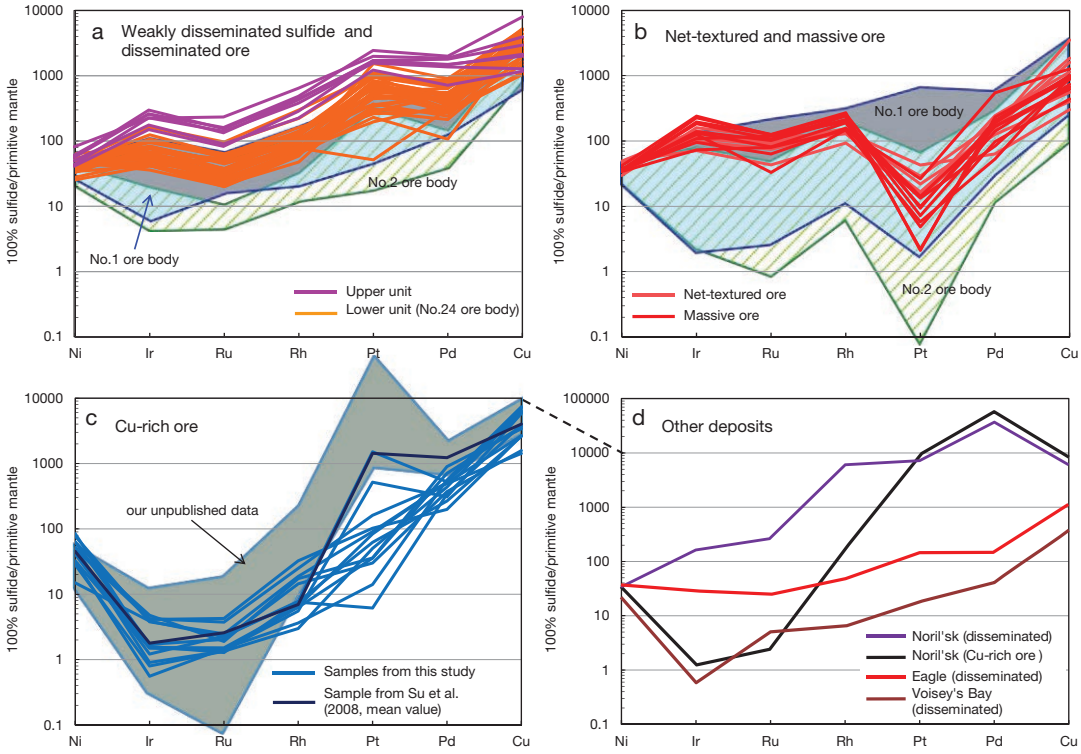

FIG. 7. Primitive-mantle normalized Ni, PGE, and Cu patterns of sulfides in the Jinchuan deposit on a 100% sulfide. Samples of the Western intrusion are from this study; Cu-rich ores are from this study and Su et al. (2008), and samples shown by the shaded area are our new unpublished data, and those of the Eastern intrusion are from Song et al. (2006, 2009), and Su et al. (2008). Primitive mantle values of metals used in the normalization are from Barnes and Maier (1999). The values of the sulfide ores of the Noril'sk-Talnakh deposits are from Barnes and Maier (1999), and those of the Voisey's Bay deposit are after Naldrett et al. (2000) and Lightfoot et al. (2012), and those of the Eagle deposit are from Ding et al. (2012).

As mentioned above, the disseminated sulfides have not undergone extensive modification due to either hydrothermal alteration or fractionation of sulfide liquid, and hence can provide additional constraints on the nature of the parental magma (Barnes and Maier, 1999). The Pd/Ir ratios of the disseminated sulfides of the No. 24 orebody are mostly between 2.5 and 24; these ratios are lower than those of sulfides segregated from basaltic magmas but within the range of typical sulfides segregated from picritic magmas (Fig. 9). Thus, we propose that the Jinchuan parental magma was probably a picritic basalt and originally contained moderate Ni (~350 ppm) and Cu (~120 ppm), and high Ir and Ru about 1 ppb, Pd and Pt about 10 ppb. These values are within the range of data from typical undepleted picritic basalts of Qeqertarssuaq, West Greenland (80–1,400 ppm Ni, 0.43–1.35 ppb Ir, 0.23–3.16 ppb Ru, and 0.26–0.58 ppb Rh, 5.7–9.4 ppb Pt, and 4.2–12.9 ppb Pd; Keays and Lightfoot, 2007) and the picrites of Tuklonsky of the Siberian Trap, Noril'sk region (295 ppm Ni, 9.0 ppb Pd, 10.5 ppb Pt; Brügmann et al., 1993; Lightfoot and Keays, 2005).

Sulfide segregation and fractionation of the Upper and Lower units

The distinct lithologic sequences and regular variations of major and trace elements concentrations of the Upper and Lower units suggest that the two units were formed by different pulses of magma and the Upper unit was formed slightly earlier than the Lower unit (Song et al., 2012). This suggestion is supported by our chalcophile elements data, which show that the sulfides of the Upper and Lower units have different PGE tenors and Cu/Pd ratios (Figs. 4, 6, 7).

The relatively low Cu/Pd ratios (5,500–14,900) of the weakly disseminated sulfides in the Upper unit suggest that they segregated from a PGE-undepleted magma (see quantitative model below). In contrast, the disseminated sulfides of the Lower unit have high Cu/Pd ratios (24,200–85,600; Figs. 6, 7a), which imply that the silicate magma in equilibrium with these sulfides had Cu/Pd ratios from ~36,000 to ~127,000 and that the sulfides formed with an R factor of 500. Such high Cu/Pd ratios indicate that these sulfides had formed from a magma that had become PGE depleted due to an earlier episode of sulfide melt extraction (Hoatson and Keays, 1989; Barnes et al., 1993). Moreover, in the plots of Pd/Y and Ru/Y ratios against MgO (Fig. 10), the disseminated sulfides in the No. 24 orebody plot in trends different from that of the weakly disseminated sulfides in the Upper unit, reenforcing the interpretation that the two units formed from two distinct magma pulses (Song et al., 2012).

Although the net-textured and massive sulfides have Cu/Pd ratios and IPGE tenors that are comparable to those of the disseminated sulfides, they have lower Pt and Pd contents and higher Ni/Cu and IPGE/Pd-group PGE (IPGE/PPGE) ratios (Figs. 6, 7b), suggestive of significant fractionation of sulfide melts. Fractionation of sulfide melts is also suggested by the

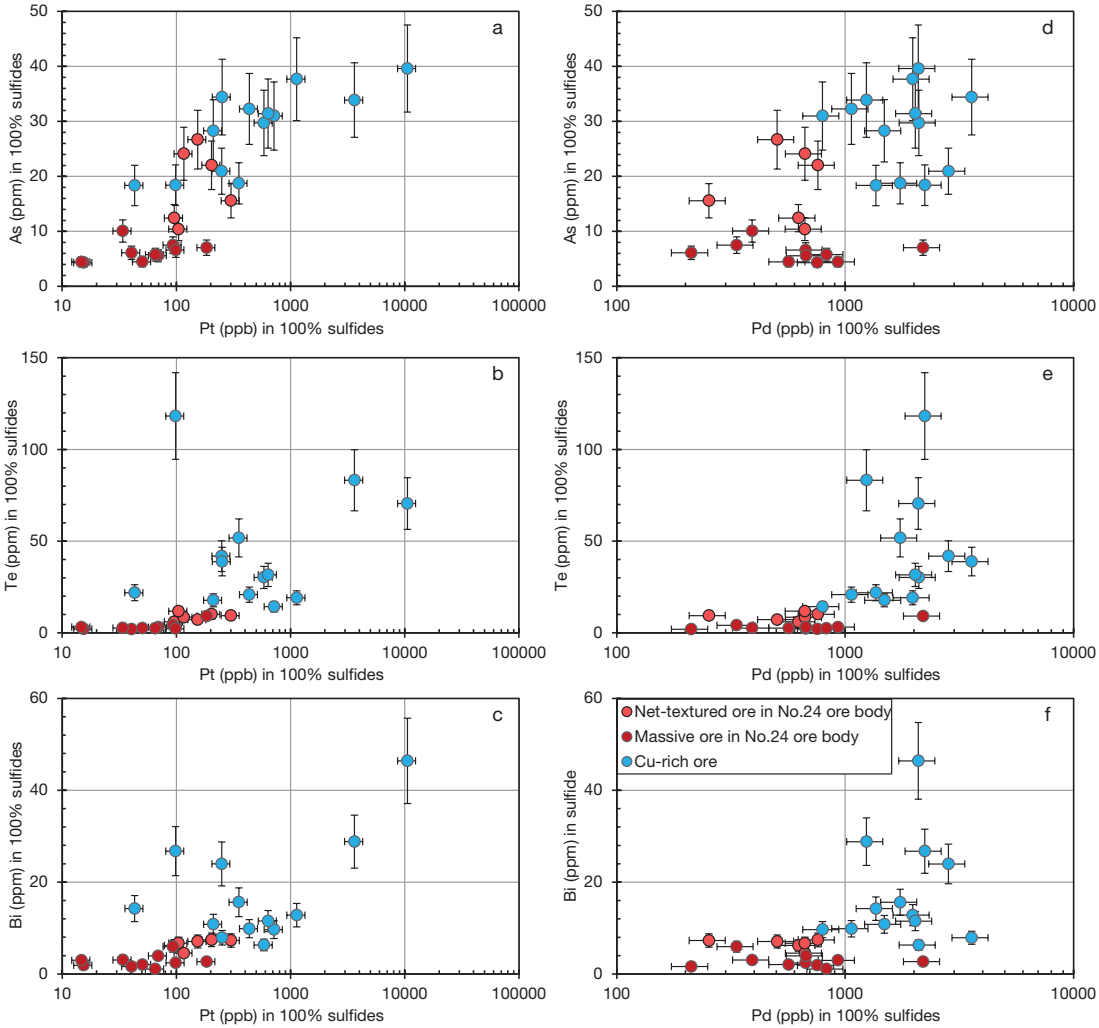

FIG. 8. Variations of Pt and Pd vs. As, Te, and Bi of the net-textured and massive sulfides of the No. 24 orebody and Cu-rich ores in 100% sulfide basis. The accumulated uncertainties in tenors of these elements are estimated as ~18% for PGE and ~20% for As, Te, and Bi, according to Kerr (2001).

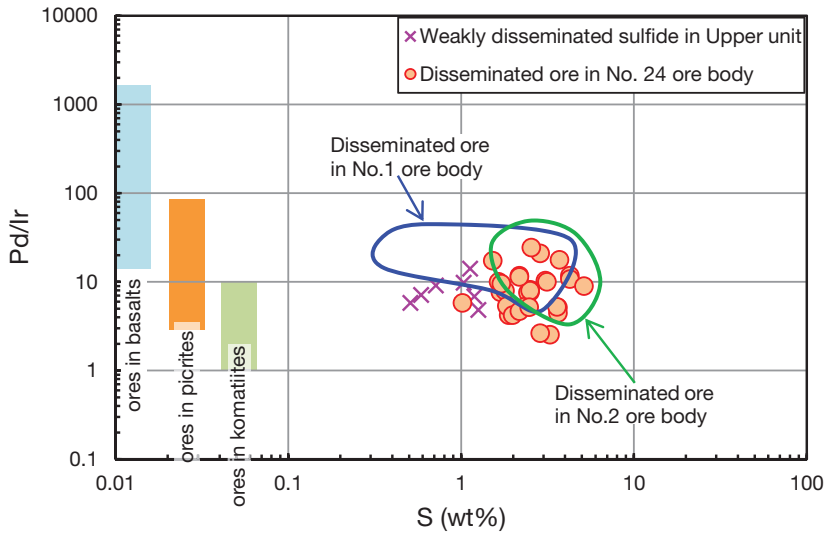

FIG. 9. Plots of S vs. Pd/Ir of the Jinchuan disseminated ores. Samples of Nos. 1 and 2 orebodies are from Song et al. (2006, 2009) and Su et al. (2008). The field of Pd/Ir of sulfide ores in basalts, picrites, and komatiites are after Maier et al. (2008).

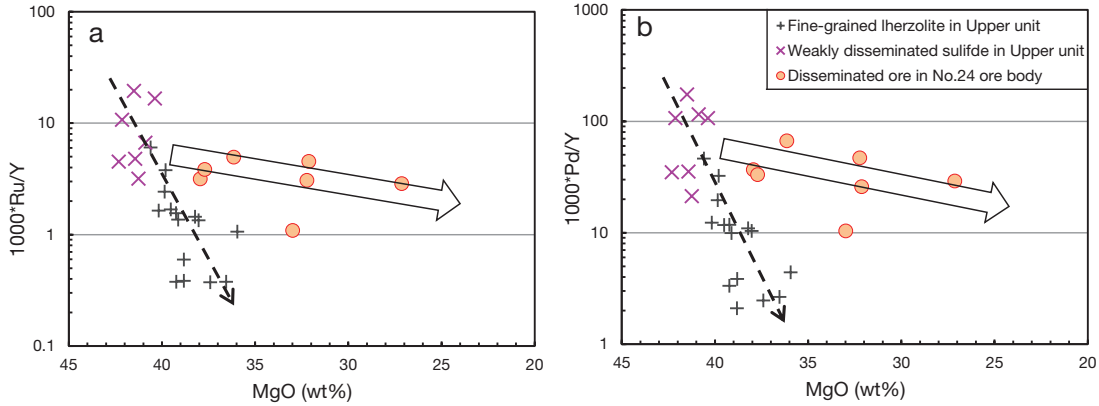

FIG. 10. Plots of MgO vs. 1,000*Ru/Y and 1,000*Pd/Y of the rocks from borehole ZK 71 at Jinchuan. Data of MgO and Y contents are from Song et al. (2012).

extremely low IPGE and Ni/Cu ratios of the Cu-rich sulfides as well as their relatively high Pt and Pd contents (Figs. 6, 7c). As mentioned above, the Cu-rich sulfides, which had been mined, have as high as 1.0 to 82 ppm Pt, 0.1 to 12 ppm Pd, 1.0 to 6.0 wt % Cu, and 0.5 to 4.2 wt % Ni (Sixth Geological Unit, 1984). These features demonstrate a genetic relationship between the net-textured and massive sulfides and the Cu-rich sulfides (Su et al., 2008; Chen, 2009; Tonnelier, 2010).

Quantitative modeling of sulfide segregation and fractionation

Sulfide segregation in the Upper unit: The compositional variations in metal tenor of sulfides (C_i^s) can be modeled in terms of a combination of parental magma composition (C_i^0) and the ratio of silicate magma to sulfide melt (R factor) ($C_i^s = C_i^0 \times D_i^{sul/sil} \times (R + 1)/(R + D_i^{sul/sil})$, $D_i^{sul/sil}$ is sulfide/silicate liquid partition coefficient; Campbell and Naldrett, 1979). Recently, Lesher and Burnham (2001) have pointed out that if a system is multicomponent (e.g., olivine and sulfides are liquidus phases) the compositions of the sulfides can be modeled using the following mass balance equation (adapted from Lesher and Burnham, 2001):

$$C_i^s = D_i^{sul/sil} \times (C_i^0 \times R + P \times X_{Ni}^0)/(R + D_i^{sul/sil} + P \times D_i^{Ol/sil}), \quad (1)$$

where C_i^s and C_i^0 represent the concentrations of the metal in the sulfide and silicate liquids, respectively; $D_i^{sul/sil}$ and $D_i^{Ol/sil}$ are the partition coefficients of metal i between sulfide and silicate liquid and between olivine and silicate liquid, respectively; R refers to the mass ratio of silicate magma/(sulfide liquid + olivine); P is the olivine:sulfide ratio (~20, Chen et al., 2009a), and X_{Ni}^0 is the initial Ni content of the olivine (~1,600 ppm, Li et al., 2004; Chen et al., 2009a).

In our calculations, $D_i^{Ol/sil}$ of Ni is assumed to be 5 (Li et al., 2003). However, we have used different values of $D_i^{sul/sil}$ of Ni, Ir, Pd, and Ru in the modeling, namely Ni = 250 or 500; Ir = 10,000 or 40,000; Pd = 25,000 or 40,000; Ru = 35,000; these values are within the range of experimental results (Francis, 1990; Peach et al., 1994; Crocket et al., 1997; Gaetani and Grove, 1997). It is further assumed that the partition coefficients remained constant during sulfide segregation, although they would have changed with changes in f_{O_2}, f_{S_2}, and the compositions of the silicate and sulfide liquids. The results are shown in Figure 11.

Our calculations indicate that the sulfide segregation trend from a picritic magma containing ~350 ppm Ni, ~1 ppb Ir, and ~10 ppb Pd gives a good match of the observed compositions of the weakly disseminated sulfide in the Upper unit (Fig. 11). This suggests that the weakly disseminated sulfides probably segregated from PGE-undepleted silicate magma at R factors of 400 to 1,000 (Fig. 11). This is consistent with their relatively high PGE tenors and low Cu/Pd ratios (5,500–14,900) which are similar to that of the primitive mantle (Fig. 6b).

Sulfide segregation in the Lower unit: As discussed above, the very high Cu/Pd ratios suggest that the disseminated sulfides in the No. 24 orebody segregated from a PGE-depleted magma due to prior sulfide separation. The chalcophile metal contents of the residual magma can be calculated by the Rayleigh equation (Neumann et al., 1954):

$$C_i^L = C_i^0 \times (1 - F)^{(Di-1)}, \quad (2)$$

in which C_i^0 and C_i^L are the metal contents of the primary and residual magma, respectively; F represents the fraction of the liquid that has crystallized; and D_i is the partition coefficient of element i between sulfide and silicate liquid.

A minor amount of sulfide segregation will result in significant chalcophile metals depletion. Equation (2) shows that after segregation of only 0.003% sulfide melt from the parental magma, the residual magma will contain only ~0.36 ppb Ir, ~0.42 ppb Ru, ~2.9 ppb Pd, and ~345 ppm Ni. The abundances of these metals are similar to the values estimated by Jiao et al. (in prep.; 0.27 ppb Ir, 0.28 ppb Ru, 4.9 ppb Pt, 2.3 ppb Pd, 340 ppm Ni, and 170 ppm Cu) and Li and Ripley (2011; 0.2 ppb Ir and 3 ppb Pd). Such a weakly PGE depleted magma has a relatively high Cu/Pd ratio, which is comparable with that of the parental magma of the disseminated sulfides of the No. 24 orebody (36,000–127,000, see above). According to equation (1), sulfides segregated from such a weakly PGE-depleted magma under R factors varying from ~200 to ~1,000 would have compositions similar to those of the disseminated sulfides (Fig. 11). Using different partition coefficients in these models, the best correlations between Ni, Ir, and Pd in these sulfides in both the Upper and Lower units are obtained setting $D_{Ni}^{sul/sil} = 500$ and $D_{Ir}^{sul/sil} = D_{Pd}^{sul/sil} =$

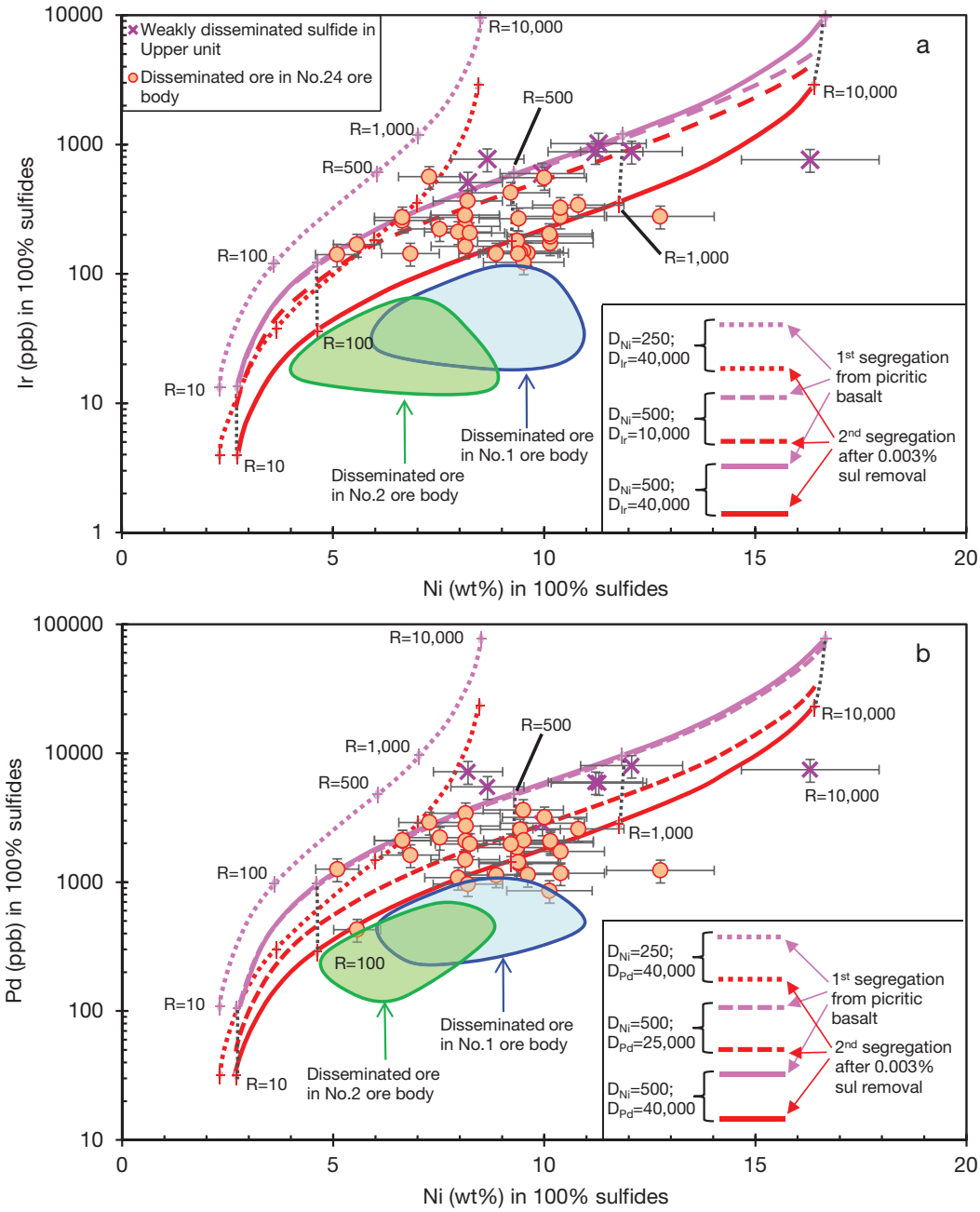

FIG. 11. Quantitative approaches of (a) Ni vs. Ir and (b) Ni vs. Pd of the disseminated sulfides from different locations at Jinchuan in 100% sulfide basis, using various combinations of partition coefficients of silicate/sulfide liquid for Ni, Ir, and Pd. The weakly disseminated sulfides in the Upper unit of the Western intrusion can be modeled by segregating from a PGE-undepleted picritic magma (~1 ppb Ir, ~10 ppb Pd, and ~350 ppm Ni) under R factors (mass ratio of silicate magma/(sulfide liquid + olivine)) of 400 to 1,000. The disseminated sulfides from the No. 24 orebody can be formed by a PGE-depleted residual magma (~0.36 ppb Ir, ~2.9 ppb Pd, and ~345 ppm Ni) due to a minor amount of sulfide melt removal at depth under R factors of 200 to 1,000. Better correlations of Ni against Ir and Pd for the disseminated sulfides from both the Upper and Lower units have been obtained by setting $D_{Ni}^{sul/sil}$ = 500, $D_{Ir}^{sul/sil}$ = $D_{Pd}^{sul/sil}$ = 40,000 in the calculation. The accumulated uncertainties in tenors of these elements are estimated as ~10% for Ni, ~18% for Ir, and Pd, according to Kerr (2001).

40,000 (Fig. 11). By contrast, the disseminated sulfides of the Nos. 1 and 2 orebodies have greater Cu/Pd ratios and were segregated from a more PGE-depleted parental magma due to larger amount of prior sulfide liquids removal (~0.006–0.008%) at depth (Song et al., 2009). Moreover, the higher PGE concentrations of the disseminated sulfides in the No. 1 orebody relative to those of the No. 2 orebody are attributed to greater R factors (Fig. 11).

The mass ratios of the silicate magma to sulfide liquid in our model are considerably lower than those suggested by Song et al. (2009). However, our estimated R values for the Jinchuan deposit are comparable to those of other sulfide-rich

Ni-Cu-(PGE) deposits, such as the Voisey's Bay deposit (R = 100–5,000, Naldrett et al., 2000; Lightfoot et al., 2012) and the Eagle deposit (R = 200–300, Ding et al., 2012). On the other hand, using a ferropicritic magma with ~700 ppm Ni, ~120 ppm Cu, ~5 ppb Pt, ~5 ppb Pd, and ~0.6 ppb Ir, Tonnelier (2010) estimated that the Jinchuan sulfides had formed at R factors of ~500 to ~800. Tonnelier (2010) attributed the low PGE contents of the parental magma of the Jinchuan magmatic system to derivation from a pyroxenitic mantle reservoir. Although this suggestion has considerable merit, it is noteworthy that the magma that formed the weakly disseminated sulfides in the Upper unit was not PGE depleted. The Cu/Pd ratios of the sulfide-barren lherzolite and samples with weakly disseminated sulfides in the Upper unit are 9,200 to 15,900 and 5,500 to 14,900 (Table 2; Fig. 4), respectively. These ratios are comparable to those of the primitive mantle (7,000–10,000, Barnes and Maier, 1999). Therefore, we propose that all the Jinchuan magmas have been derived from a peridotitic mantle reservoir and the PGE-depleted signature of some of the Jinchuan sulfides is due to an earlier sulfide saturation event.

Sulfide fractionation in the Western intrusion: Decoupling between IPGE and PPGE and between Ni and Cu of the net-textured and massive ores and Cu-rich ores in the Western intrusion as shown in Figure 6 may be the result of fractional crystallization of mss. To test this possibility, we have used the Rayleigh equation (2) to model the fractionation of Ni, Pd, and Ru between mss and a sulfide melt using the mss/sulfide melt partition coefficients of $D_{Ni}^{mss/Sul}$ = 0.6, $D_{Pd}^{mss/Sul}$ = 0.14, and $D_{Ru}^{mss/Sul}$ = 9 (Li et al., 1996; Ballhaus et al., 2001; Barnes et al., 2001; Brenan et al., 2003; Bockrath et al., 2004). It was assumed that the partition coefficients remained constant during fractionation.

For modeling the effects of fractionation of the sulfide melt that formed the sulfides of the No. 24 orebody, we utilized an initial sulfide melt composition of 9.9 wt % Ni, 250 ppb Ru, and 1,700 ppb Pd. This would have been the composition of sulfides which had segregated from the PGE-depleted magma at an R factor of ~600 (Fig. 12). Our calculations indicate that 30% fractional crystallization of this sulfide melt would produce a residual sulfide melt with Ni/(1,000*Ru) and Pd/Ru ratios of 8,000 and 160, respectively, and mss cumulates with Ni/(1,000*Ru) and Pd/Ru ratios of 530 and 2.5, respectively (Fig. 12). The Ni/(1,000*Ru) and Pd/Ru ratios of the net-textured and massive sulfides indicate that they formed by ~20 to 30% fractionation of the sulfide melt, whereas those of the Cu-rich ores indicate that they were formed by ~20 to ~40% fractionation of the sulfide melt (Fig. 12). These results are comparable with those of Jiao et al. (in prep.). On the other hand, the net-textured sulfides in the Nos. 1 and 2 orebodies were formed by slightly limited fractionation of sulfide liquid (0–30%) compared to those of the No. 24 orebody (Tonnelier,

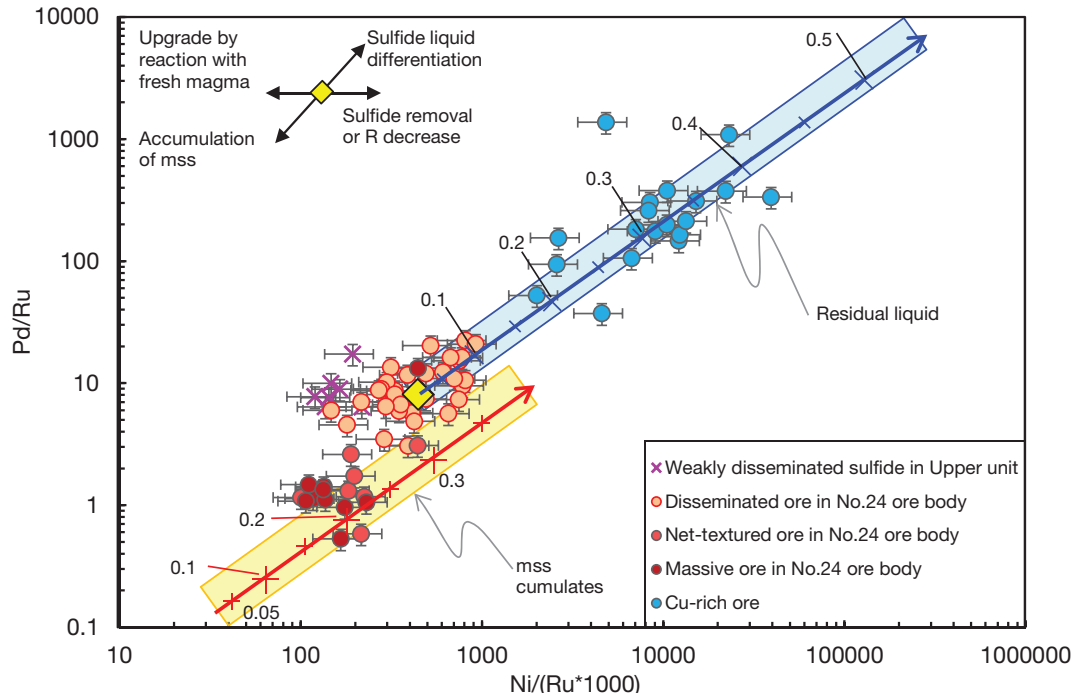

FIG. 12. Model calculations for fractional crystallization of the sulfide melt. Monosulfide solid liquid cumulates and residual liquid trends are calculated using the Rayleigh equation (ticks with numbers, like 0.2, represent degree of fractionation of sulfide melts). Initial compositions of the sulfide liquid (yellow rhombus) are assumed to contain 9.9 wt % Ni, 250 ppb Ru, and 1,700 ppb Pd, which is segregated from the weakly PGE-depleted magma at an R factor of ~600. The compositions of mss cumulate (light yellow area) and residual sulfide liquid (blue area) fall in small ranges in the plot of Ni/Ru vs. Pd/Ru by using a random number of $D_i^{mss/Sul}$ values within experimental results ($D_{Ni}^{mss/Sul}$ = ~0.6–1.0; $D_{Pd}^{mss/Sul}$ = ~0.14–0.24; $D_{Ru}^{mss/Sul}$ = ~4.2–9.0). The most coincident correlations for the mss and residual sulfide liquid (red and blue solid lines, respectively) are obtained under $D_{Ni}^{mss/Sul}$ = 0.6; $D_{Pd}^{mss/Sul}$ = 0.14; $D_{Ru}^{mss/Sul}$ = 9.0. The net-textured and massive sulfides are roughly consistent with mss cumulates, these ratios of Cu-rich sulfides match those of residual liquid well, whereas the disseminated sulfides of the Lower unit plot near the initial sulfide liquid. The accumulated uncertainties are estimated as ~30% for Ni/(Ru*1,000) ratios and ~20% for Pd/Ru ratios.

2010). The restricted variations in Ni/(1,000*Ru) and Pd/Ru ratios of the weakly disseminated sulfides in the Upper unit and the disseminated ores of the No. 24 orebody imply that they underwent only limited fractional crystallization of the sulfide melts (Fig. 12).

Origin of Pt depletion in the net-textured and massive sulfides

A remarkable characteristic of the net-textured and massive sulfides is variable Pt depletion relative to the other PGE, with Pt/Pd ratios as low as ~0.02 (Figs. 6f, 7b). Similar Pt depletions of massive sulfides are reported for other mafic-ultramafic intrusion-hosted deposits, such as those in the Selkirk and Phoenix, the Tati and Selebi-Phikwe belts of eastern Botswana (Maier et al., 2008), and in komatiite-hosted orebodies, including the Silver Swan and the White Swan deposits and the Mount Keith nickel deposit, Yilgarn craton, Western Australia (Barnes, 2004; Barnes et al., 2012). Song et al. (2009) suggested that the similar Pt depletion in the Nos. 1 and 2 orebodies probably resulted from either precipitation of Pt-Fe alloys together with chromite prior to sulfide saturation or selected removal of Pt from the sulfides due to late hydrothermal alteration. Su et al. (2008) favored that the decoupling of Pd and Pt in the net-textured and massive ores originated from postmagmatic hydrothermal processes. However, Pd is much more soluble than Pt and is easier to be dissolved and remobilized by hydrothermal fluids (Keays et al., 1981; Wood et al., 1992; Xiong and Wood, 2000; Barnes and Liu, 2012). As a result, both segregation of Pt-Fe alloys prior to sulfide saturation and postmagmatic hydrothermal redistribution of PGE would have produced negative Pt anomalies in the disseminated sulfides, Cu-rich ores as well as the net-textured and massive sulfides. As this is not the case, an alternate explanation is required.

Segregation of a Cu-rich melt from the mss during solidification of the sulfide melts may offer a credible explanation. Iridium, Ru, and Rh are concentrated in the mss because they have high mss/sulfide melt partition coefficients (~10.0, ~9.0, and ~3.0, respectively); whereas Pd and Pt remain in the residual sulfide melt because they have partition coefficients of 0.14 and 0.12, respectively (Li et al., 1996; Ballhaus et al., 2001; Barnes et al., 2001; Brenan et al., 2003; Bockrath et al., 2004). The Cu-rich orebodies that occur toward the base of the No. 24 orebody as well as in the footwall schists have highly elevated Pd and Pt contents (Figs. 5, 7). Segregation of Pd and Pt into a Cu-rich sulfide melt would not, however, explain why it is only Pt that exhibits a negative anomaly rather than Pd and Pt. Although only a few of the Cu-rich ores in the present study display positive Pt anomalies (Fig. 7c), previous published data and our new analyses have shown that the Cu-rich ores can be highly enriched in both Pt and Pd, and have Pt/Pd ratios of 3.0 to 44.8 (Fig. 7c; Sixth Geological Unit, 1984; our unpub. data).

Experimental studies have revealed that Pt and Pd are preferentially concentrated in As-, Sb-, Bi-, and Te-enriched residual melts during crystallization of mss (Skinner et al., 1976; Makovicky, 2002; Hanley, 2007; Tomkins, 2010). The dominant discrete mineral of Pt in No. 24 orebody is sperrylite ($PtAs_2$), and the next most common Pt mineral is moncheite ($PtTe_2$) (Sixth Geological Unit, 1984; Yang et al., 2006; Su et al., 2008); however, over 70% of Pd occurs in pentlandite (Chai et al., 1993). The positive correlations between Pt and As, Te and Bi in all sulfide types in the Western intrusion are much better than those between Pd and As, Te and Bi, implying that Pt has a stronger chemical affinity with As, Te, and Bi than Pd does (Fig. 8). This suggests that Pt may have been preferentially extracted into the Cu-rich melts due to the presence of As, Te, and Bi in those melts.

Another possibility is that the negative Pt anomaly was caused by the crystallization of sperrylite prior to solidification of the sulfide melts. Several studies have demonstrated that sperrylite can crystallized directly from a sulfide melt before mss crystallization in magmatic sulfide systems (Wood, 2003; Dare et al., 2010; Helmy et al., 2010, and references therein). However, this would require that the sulfide melts that formed the net-textured and massive sulfides migrated away from sperrylite subsequent to the crystallization of the sperrylite.

Genetic model for the magmatic sulfide mineralization in the Western intrusion and conclusions

Previous studies have shown that the wall rocks at Jinchuan are poor in S and thus sulfide immiscibility occurred at a deep level (e.g., Ripley et al., 2005). We have concluded that the parental magmas that formed the Upper and Lower units of the Western intrusion experienced different evolution processes in the deeper levels of the magma plumbing system. We propose that the weakly disseminated sulfides at the base of the Upper unit formed by settling of the sulfide droplets together with olivine crystals carried by the magmas from the deeper levels. These sulfides segregated from PGE-undepleted magma under R factors of 400 to 1,000.

In contrast, the sulfides in the Lower unit segregated from PGE-depleted magma under R factors of 200 to 1,000 and thus have high Cu/Pd ratios and relatively low PGE tenors. The PGE-depleted magma resulted from a minor amount (e.g., ~0.003%) of prior sulfide separation. The net-textured and massive ores of the No. 24 orebody represent the mixture of crystallized mss and sulfide liquid and thus have relatively high IPGE contents and low Pd/Ru values. In contrast, the Cu-rich orebodies were produced from Cu-, Pd-, and Pt-rich melts that migrated away from the mss formed during the solidification of the sulfide melts that produced the net-textured and massive sulfides; as a result, the Cu-rich ores have relatively low IPGE contents and high Pd/Ru values.

We propose the Pt depletion of the net-textured and massive ores was associated with the fractional crystallization of Cu-rich sulfide liquids, which migrated away from the mss during solidification of the sulfides melts from which these ores formed. We suggest that although Pd and Pt have very small mss/sulfide melt partition coefficients, Pt was preferentially removed in the Cu-rich residual melt due to the presence of As, Te, and Bi.

Acknowledgments

This study is supported by National Science Foundation of China projects (40973038, 41003022, 41172090) and a Research Fund from SKLODG (SKLODG-ZY125-06). We are grateful to L. Qi and Y. Huang for their kind help on analyses of PGE contents. A.J. Naldrett is appreciated for his kind

suggestions on earlier version of this manuscript. We acknowledge C.M. Lesher, S.G. Su, and the Editor of this volume, Steve Barnes, for their constructive and thoughtful reviews that have greatly improved this manuscript. Many thanks are due to J.G. Jiao for sharing his manuscript in this volume. We also thankful for the assistance of D.-H. Ba, F.-G. Qiao, and J.-P. Jiang during the fieldwork.

REFERENCES

Ballhaus, C., Tredoux, M., and Spath, A., 2001, Phase relations in the Fe-Ni-Cu-PGE-S system at magmatic temperature and application to massive sulphide ores of the Sudbury Igneous Complex: Journal of Petrology, v. 42, p. 1911–1926.

Barnes, S.J., 2004, Komatiites and nickel sulfide ores of the Black Swan area, Yilgarn craton, Western Australia. 4. Platinum group element distribution in the ores, and genetic implications: Mineralium Deposita, v. 39, p. 752–765.

Barnes, S.J., and Liu, W., 2012, Pt and Pd mobility in hydrothermal fluids: Evidence from komatiites and from thermodynamic modelling: Ore Geology Reviews, v. 44, p. 49–58.

Barnes, S.J., Fiorentini, M.L., and Fardon, M.C., 2012, Platinum group element and nickel sulfide ore tenors of the Mount Keith nickel deposit, Yilgarn craton, Australia: Mineralium Deposita, v. 47, p. 129–150.

Barnes, S.-J., and Maier, W., 1999, The fractionation of Ni, Cu and the noble metals in silicate and sulphide liquids, *in* Keays, R.R., Lesher, C.M., Lightfoot, P.C., and Farrow, C.E.G., eds., Dynamic processes in magmatic ore deposits and their application to mineral exploration: Geological Association of Canada Short Course Notes, p. 69–106.

Barnes, S.-J., Couture, J.F., Sawyer, E.W., and Bouchaib, C., 1993, Nickel-copper occurrences in the Belleterre-Angliers belt of the Pontiac subprovince and the use of Cu-Pd ratios in interpreting platinum-group element distributions: Economic Geology, v. 88, p. 1402–1418.

Barnes, S.-J., Melezhik, V.A., and Sokolov, S.V., 2001, The composition and mode of formation of the Pechenga nickel deposits, Kola Peninsula, northwestern Russia: Canadian Mineralogist, v. 39, p. 447–471.

Bockrath, C., Ballhaus, C. and Holzheid, A., 2004, Fractionation of the platinum-group elements during mantle melting: Science, v. 305, p. 1951–1953.

Brenan, J.M., McDonough, W.F., and Dalpe, C., 2003, Experimental constraints on the partitioning of rhenium and some platinum-group elements between olivine and silicate melt: Earth and Planetary Science Letters, v. 212, p. 135–150.

Brügmann, G.E., Naldrett, A.J., Asif, M., Lightfoot, P.C., Gorbachev, N.S., and Fedorenko, V.A., 1993, Siderophile and chalcophile metals as tracers of the evolution of the Siberian Trap in the Noril'sk region, Russia: Geochimica et Cosmochimica Acta, v. 57, p. 2001–2018.

Campbell, I.H., and Naldrett, A.J., 1979, The influence of silicate:sulfide ratios on the geochemistry of magmatic sulfides: Economic Geology, v. 74, p. 1503–1506.

Chai, G., and Naldrett, A.J., 1992a, Characteristics of Ni-Cu-PGE mineralization and genesis of the Jinchuan deposit, Northwest China: Economic Geology, v. 87, p. 1475–1495.

——1992b, The Jinchuan ultramafic intrusion: Cumulate of a high-Mg basaltic magma: Journal of Petrology, v. 33, p. 277–303.

Chai, G., Naldrett, A.J., Rucklidge, J.C., and Kilius, L.R., 1993, In situ quantitative analyses for PGE and Au in sulfide minerals of the Jinchuan Ni-Cu deposit by accelerator mass spectrometry: Canadian Mineralogist, v. 31, p. 19–30.

Chen, L.M., 2009, Features and genesis of Segment I and its hosted Ni-Cu sulfide deposits of the Jinchuan intrusion, Gansu Province: Unpublished Ph.D. thesis, Guiyang, Graduate University of Chinese Academy of Sciences, 143 p.

Chen, L.M., Song, X.Y., Danyushevsky L. V., Xiao, J.F., Li, S.B., and Guan, J.X., 2009a, Correlation between Ni and MgO contents of olivine in Segment I of the Jinchuan intrusion, NW China, and its geological implication: Acta Petrologica Sinica, v. 25, p. 3369–3378 (in Chinese with English abs.).

Chen, L.M., Song, X.Y., Danyushevsky L. V., D., Xiao, J.F., Zhu, D., Zhou, G.F., Guan, J.X., Liu, S.R., and Zheng, W.Q., 2009b, MELTS thermodynamic calculation of compositions of parental magma and fractional crystallization of the Jinchuan intrusion, Gansu Province: Acta Geologica Sinica, v. 83, p. 1302–1315 (in Chinese with English abs.).

Crocket, J.H., Fleet, M.E., and Stone, W.E., 1997, Implications of composition for experimental partitioning of platinum-group elements and gold between sulfide liquid and basalt melt: The significance of nickel content: Geochimica et Cosmochimica Acta, v. 61, p. 4139–4149.

Dare, S.A.S., Barnes, S.-J., Prichard, H.M., and Fisher, P.C., 2010, The timing and formation of platinum group minerals from the Creighton Ni-Cu-platinum group element sulfide deposit, Sudbury, Canada: Early crystallization of PGE-rich sulfarsenides: Economic Geology, v. 105, p. 1071–1096.

de Waal, S.A., Xu, Z.G., Li, C.S., and Mouri, H., 2004, Emplacement of viscous mushes in the Jinchuan ultramafic intrusion, western China: Canadian Mineralogist, v. 42, p. 371–392.

Ding, X., Ripley, E., and Li, C., 2012, PGE geochemistry of the Eagle Ni-Cu-(PGE) deposit, Upper Michigan: Constraints on ore genesis in a dynamic magma conduit: Mineralium Deposita, v. 47, p. 89–104.

Francis, R.D., 1990, Sulfide globules in mid-ocean ridge basalts (MORB), and the effect of oxygen abundance in Fe-S-O liquids on the ability of those liquids to partition metals from MORB and komatiite magmas: Chemical Geology, v. 85, p. 199–213.

Gaetani, G.A., and Grove, T.L., 1997, Partitioning of moderately siderophile elements among olivine, silicate melt, and sulfide melt: Constraints on core formation in the Earth and Mars: Geochimica et Cosmochimica Acta, v. 61, p. 1829–1846.

Hanley, J.J., 2007, The role of arsenic-rich melts and mineral phases in the development of high-grade Pt-Pd mineralization within komatiite-associated magmatic Ni-Cu sulfide horizons at Dundonald Beach South, Abitibi subprovince, Ontario, Canada: Economic Geology, v. 102, p. 305–317.

Hanski, E.J., and Smolkin, V.F., 1995, Iron- and LREE-enriched mantle source for early Proterozoic intraplate magmatism as exemplified by the Pechenga ferropicrites, Kola Peninsula, Russia: Lithos, v. 34, p. 107–125.

Helmy, H.M., Ballhaus, C., Wohlgemuth-Ueberwasser, C., Fonseca, R.O.C., and Laurenz, V., 2010, Partitioning of Se, As, Sb, Te and Bi between monosulfide solid solution and sulfide melt—application to magmatic sulfide deposits: Geochimica et Cosmochimica Acta, v. 74, p. 6174–6179.

Hoatson, D.M., and Keays, R.R., 1989, Formation of platiniferous sulfide horizons by crystal fractionation and magma mixing in the Munni Munni layered intrusion, West Pilbara block, Western Australia: Economic Geology, v. 84, p. 1775–1804.

Jackson, S.E., Fryer, B.J., Gosse, W., Healey, D.C., Longerich, H.P., and Strong, D.F., 1990, Determination of the precious metals in geological materials by inductively coupled plasma-mass spectrometry (ICP-MS) with nickel sulphide fire-assay collection and tellurium coprecipitation: Chemical Geology, v. 83, p. 119–132.

Jinchuan Nonferrous Metal Corporation (JNMC), 1997, Study on the geological features and mineralization of the unexposed Cu-rich orebody in Segment I at Jinchuan: Unpublished (in Chinese).

——2003, The final report of the engineering geology at 1160 level on I-8 exploration line of Segment I: Unpublished (in Chinese).

Keays, R.R., and Lightfoot, P.C., 2007, Siderophile and chalcophile metal variations in Tertiary picrites and basalts from West Greenland with implications for the sulphide saturation history of continental flood basalt magmas: Mineralium Deposita, v. 42, p. 319–336.

Keays, R.R., Ross, J.R., and Woolrich, P., 1981, Precious metals in volcanic peridotite-associated nickel sulfide deposits in Western Australia. II. Distribution within the ores and host rocks at Kambalda: Economic Geology, v. 76, p. 1645–1674.

Kerr, A., 2001, The calculation and use of sulfide metal contents in the study of magmatic ore deposits: A methodological analysis: Exploration and Mining Geology, v. 10, p. 289–301.

Lehmann, J., Arndt, N., Windley, B., Zhou, M.F., Wang, C.Y., and Harris, C., 2007, Field relationships and geochemical constraints on the emplacement of the Jinchuan intrusion and its Ni-Cu-PGE sulfide deposit, Gansu, China: Economic Geology, v. 102, p. 75–94.

Lesher, C.M., and Burnham, O.M., 2001, Multicomponent elemental and isotopic mixing in Ni-Cu-(PGE) ores at Kambalda, Western Australia: Canadian Mineralogist, v. 39, p. 421–446.

Li, C., and Ripley, E.M., 2011, The giant Jinchuan Ni-Cu-(PGE) deposit: Tectonic setting, magma evolution, ore genesis and exploration implications: Reviews in Economic Geology, v. 17, p. 163–180.

Li, C., Barnes, S.-J., Makovicky, E., Rose-Hansen, J., and Makovicky, M., 1996, Partitioning of nickel, copper, iridium, rhenium, platinum, and palladium between monosulfide solid solution and sulfide liquid: Effects of composition and temperature: Geochimica et Cosmochimica Acta, v. 60, p. 1231–1238.

Li, C., Ripley, E.M., and Mathez, E.A., 2003, The effect of S on the partitioning of Ni between olivine and silicate melt in MORB: Chemical Geology, v. 201, p. 295–306.

Li, C., Xu, Z., Sybrand, A.W., Edward, M.R., and Wolfgang, D.M., 2004, Compositional variations of olivine from the Jinchuan Ni-Cu sulfide deposit, western China: Implications for ore genesis: Mineralium Deposita, v. 39, p. 159–172.

Li, X.H., Su, L., Chung, S.L., Li, Z.X., Liu, Y., Song, B., and Liu, D.Y., 2005, Formation of the Jinchuan ultramafic intrusion and the world's third largest Ni-Cu sulfide deposit: Associated with approximately 825 Ma south China mantle plume?: Geochemistry, Geophysics, Geosystems, v. 6, p. Q1104, dio:10.1029/2005GC001006.

Lightfoot, P.C., and Keays, R.R., 2005, Siderophile and chalcophile metal variations in flood basalts from the Siberian trap, Noril'sk region: Implications for the origin of the Ni-Cu-PGE sulfide ores: Economic Geology 100th Anniversary Volume, p. 439–462.

Lightfoot, P., Keays, R., Evans-Lamswood, D., and Wheeler, R., 2012, S saturation history of Nain Plutonic Suite mafic intrusions: Origin of the Voisey's Bay Ni-Cu-Co sulfide deposit, Labrador, Canada: Mineralium Deposita, v. 47, p. 23–50.

Maier, W.D., Barnes, S.J., Chinyepi, G., Barton, J.M., Eglington, B., and Setshedi, I., 2008, The composition of magmatic Ni-Cu-(PGE) sulfide deposits in the Tati and Selebi-Phikwe belts of eastern Botswana: Mineralium Deposita, v. 43, p. 37–60.

Makovicky, E., 2002, Ternary and quaternary phase systems with PGE: Canadian Institute of Mining, Metallurgy and Petroleum Special Volume 54, p. 131–175.

Naldrett, A., and Duke, J., 1980, Platinum metals magmatic sulfide ores: Science, v. 208, p. 1417–1424.

Naldrett, A.J., Asif, M., Gorbachev, N.S., Kunilov, V.E., Fedorenko, V.A., and Lightfoot, P.C., 1994, The composition of the Ni-Cu ores of the Noril'sk region: Ontario Geological Survey Special Publication 5, p. 357–372.

Naldrett, A.J., Fedorenko, V.A., Lightfoot, P.C., Kunilov, V.I., Gorbachev, N.S., Doherty, W., and Johan, Z., 1995, Ni-Cu-PGE deposits of Noril'sk region, Siberia: Their formation in conduits for flood basalt volcanism: Transactions of the Institution of Mining and Metallurgy, sec. B, v. 104, p. 18–36.

Naldrett, A.J., Asif, M., Krstic, S., and Li, C.S., 2000, The composition of mineralization at the Voisey's Bay Ni-Cu sulfide deposit, with special reference to platinum-group elements: Economic Geology, v. 95, p. 845–865.

Neumann, H., Mead J., and Vitaliano C.J., 1954, Trace element variation during fractional crystallization as calculated from the distribution law: Geochimica et Cosmochimica Acta, v. 6, p. 90–99.

Peach, C.L., Mathez, E.A., Keays, R.R., and Reeves, S.J., 1994, Experimentally determined sulfide melt-silicate melt partition-coefficients for iridium and palladium: Chemical Geology, v. 117, p. 361–377.

Qi, L., Zhou, M.F., and Wang, C.Y., 2004, Determination of low concentrations of platinum group elements in geological samples by ID-ICP-MS: Journal of Analytical Atomic Spectrometry, v. 19, p. 1335–1339.

Qi, L., Zhou, M.F., Yan, Z.F., Pi, D.H., and Hu, J., 2006, An improved Carius tube technique for digesting geological samples in the determination of PGEs and Re by ICP-MS: Geochimica, v. 35, p. 667–674.

Ripley, E.M., Sarkar, A., and Li, C., 2005, Mineralogic and stable isotope studies of hydrothermal alteration at the Jinchuan Ni-Cu deposit, China: Economic Geology, v. 100, p. 1349–1361.

Sixth Geological Unit (SGU), 1981, Final exploration report of Segment I in the Baijiazuizi Cu-Ni deposit: Sixth Geological Unit, Geological Survey of Gansu Province, Unpublished (in Chinese).

——1984, Geology of the Baijiaozuizi Cu-Ni sulfide deposit: Beijing Geological Survey of Gansu Province, Sixth Geological Unit, Geological Publishing House (in Chinese).

Skinner, B.J., Luce, F.D., Dill, J.A., Ellis, D.E., Hagan, H.A., Lewis, D.M., Odell, D.A., Sverjensky, D.A., and Williams, N., 1976, Phase relations in ternary portions of the system Pt-Pd-Fe-As-S: Economic Geology, v. 71, p. 1469–1475.

Song, X.Y., Zhou, M.F., Wang, C.Y., Qi, L., and Zhang, C.J., 2006, Role of crustal contamination in formation of the Jinchuan intrusion and its world-class Ni-Cu-(PGE) sulfide deposit, northwest China: International Geology Review, v. 48, p. 1113–1132.

Song, X.Y., Zhou, M.F., Tao, Y., and Xiao, J.F., 2008, Controls on the metal compositions of magmatic sulfide deposits in the Emeishan large igneous province, SW China: Chemical Geology, v. 253, p. 38–49.

Song, X.Y., Keays, R.R., Zhou, M.F., Qi, L., Ihlenfeld, C., and Xiao, J.F., 2009, Siderophile and chalcophile elemental constraints on the origin of the Jinchuan Ni-Cu-(PGE) sulfide deposit, NW China: Geochimica et Cosmochimica Acta, v. 73, p. 404–424.

Song, X.Y., Danyushevsky, L.V., Keays, R.R., Chen, L.-M., Wang, Y.-S., Tian, Y.-L., and Xiao, J.-F., 2012, Structural, lithological, and geochemical constraints on the dynamic magma plumbing system of the Jinchuan Ni-Cu sulfide deposit, NW China: Mineralium Deposita, v. 47, p. 277–297.

Su, S., Li, C., Zhou, M.F., Ripley, E., and Qi, L., 2008, Controls on variations of platinum-group element concentrations in the sulfide ores of the Jinchuan Ni-Cu deposit, western China: Mineralium Deposita, v. 43, p. 609–622.

Tang, Z.L., and Li, W.Y., 1995, Mineralization model and geology of the Jinchuan deposit bearing PGE: Beijing, Geological Publishing House, 208 p. (in Chinese).

Tomkins, A.G., 2010, Wetting facilitates late-stage segregation of precious metal-enriched sulfosalt melt in magmatic sulfide systems: Geology, v. 38, p. 951–954.

Tonnelier, N.J., 2010, Geology and genesis of the Jinchuan Ni-Cu-(PGE) deposit, China: Unpublished Ph.D. thesis, Sudbury, Canada, Laurentian University, 192 p.

Wager, L.R., Brown, G.M., and Wadsworth, W.J., 1960, Types of igneous cumulates: Journal of Petrology, v. 1, p. 73–85.

Wood, M., 2003, Arsenic in igneous systems: An experimental investigation: Unpublished B.Sc. thesis, Toronto, Ontario, Canada, University of Toronto, 32 p.

Wood, S.A., Mountain, B.W., and Pan, P., 1992, The aqueous geochemistry of platinum, palladium and gold: Recent experimental constraints and a re-evaluation of theoretical predictions: Canadian Mineralogist, v. 30, p. 955–982.

Xiong, Y., and Wood, S.A., 2000, Experimental quantification of hydrothermal solubility of platinum-group elements with special reference to porphyry copper environments: Mineralogy and Petrology, v. 68, p. 1–28.

Yang, S.H., Qu, W.J., Tian, Y.L., Chen, J.F., Yang, G., and Du, A.D., 2008, Origin of the inconsistent apparent Re-Os ages of the Jinchuan Ni-Cu sulfide ore deposit, China: Post-segregation diffusion of Os: Chemical Geology, v. 247, p. 401–418.

Yang, X.Z., Ishihara, S., and Zhao, D.H., 2006, Genesis of the Jinchuan PGE deposit, China: Evidence from fluid inclusions, mineralogy and geochemistry of precious elements: Mineralogy and Petrology, v. 86, p. 109–128.

Zhang, M., Kamo, S., Li, C., Hu, P., and Ripley, E., 2010, Precise U-Pb zircon-baddeleyite age of the Jinchuan sulfide ore-bearing ultramafic intrusion, western China: Mineralium Deposita, v. 45, p. 3–9.

Zhou, M.F., Yang, Z.X., Song, X.Y, Lesher, C.M., and Keays, R.R., 2002, Magmatic Ni-Cu-(PGE) sulphide deposits in China: Canadian Institute of Mining, Metallurgy and Petroleum Special Volume 54, p. 619–636.